Vegetative Incompatibility Loci with Dedicated Roles in Allorecognition Restrict Mycovirus Transmission in Chestnut Blight Fungus

Dong-Xiu Zhang,* Martin J. Spiering,* Angus L. Dawe,† and Donald L. Nuss*,[1]
*Institute for Bioscience and Biotechnology Research, University of Maryland, Rockville, Maryland 20850, and †Department of Biology and Molecular Biology Program, New Mexico State University, Las Cruces, New Mexico 88003

ABSTRACT Vegetative incompatibility (*vic*), a form of nonself allorecognition, operates widely in filamentous fungi and restricts transmission of virulence-attenuating hypoviruses in the chestnut blight fungus *Cryphonectria parasitica*. We report here the use of a polymorphism-based comparative genomics approach to complete the molecular identification of the genetically defined *C. parasitica vic* loci with the identification of *vic1* and *vic3*. The *vic1* locus in the *C. parasitica* reference strain EP155 consists of a polymorphic HET-domain-containing 771-aa ORF designated *vic1a-2*, which shares 91% identity with the corresponding *vic1a-1* allele, and a small (172 aa) idiomorphic DUF1909-domain-containing ORF designated *vic1b-2* that is absent at the *vic1-1* locus. Gene disruption of either *vic1a-2* or *vic1b-2* in strain EP155 eliminated restrictions on virus transmission when paired with a *vic1* heteroallelic strain; however, only disruption of *vic1a-2* abolished the incompatible programmed cell death (PCD) reaction. The *vic3* locus of strain EP155 contains two polymorphic ORFs of 599 aa (*vic3a-1*) and 102 aa (*vic3b-1*) that shared 46 and 85% aa identity with the corresponding *vic3a-2* and *vic3b-2* alleles, respectively. Disruption of either *vic3a-1* or *vic3b-1* resulted in increased virus transmission. However, elimination of PCD required disruption of both *vic3a* and *vic3b*. Additional allelic heterogeneity included a sequence inversion and a 8.5-kb insertion containing a LTR retrotransposon sequence and an adjacent HET-domain gene at the *vic1* locus and a 7.7-kb sequence deletion associated with a nonfunctional, pseudo *vic* locus. Combined gene disruption studies formally confirmed restriction of mycovirus transmission by five *C. parasitica vic* loci and suggested dedicated roles in allorecognition. The relevance of these results to the acquisition and maintenance of *vic* genes and the potential for manipulation of *vic* alleles for enhanced mycovirus transmission are discussed.

ALLORECOGNITION genetic systems, which provide the ability to distinguish self from nonself, play important functional roles in microbial and multicellular organisms. These systems range from restriction endonucleases in bacteria (Meselson and Yuan 1968) to somatic histocompatibility in protocordates (De Tomaso *et al.* 2005), self-infertility in plants (Nasrallah 2005), and innate immunity in vertebrates (Medzhitov and Janeway 2002) (reviewed by Aanen *et al.* 2008; Nydam and De Tomaso 2011; Rosengarten and Nicotra 2011). Allorecognition operates widely in filamentous fungi in both the sexual and the vegetative growth phases (Saupe 2000). The role of the mating-type locus in controlling sexual recognition and promoting outbreeding in yeast and filamentous fungi is well understood (reviewed by Coppin *et al.* 1997). It is also known that somatic or vegetative fusion of fungal cells (termed "anastomosis") occurs at a high frequency within and between individuals promoting network formation (Rayner 1996) and facilitating foraging, the pooling of resources (Rayner 1996), and the introduction of genetic variation via the parasexual cycle (Pontecorvo 1956). However, most fusion events between genetically distinct individuals of the same species result in

doi: 10.1534/genetics.114.164574
Manuscript received January 28, 2014; accepted for publication March 27, 2014; published Early Online April 1, 2014.
Supporting information is available online at http://www.genetics.org/lookup/suppl/doi:10.1534/genetics.114.164574/-/DC1.
Sequence data from this article have been deposited with GenBank under the following accession numbers: for the candidate *vic* genes—*vic1a-1*, HG799041; *vic1a-2*, HG799042; *vic1b-2*, HG799043; *vic1c-1*, HG799048; *vic1d-1*, HG799049; *vic3a-1*, HG799044; *vic3a-2*, HG799045; *vic3b-1*, HG799046; *vic3b-2*, HG799047; for the pseudo *vic* HET-domain gene—HG799050; and for the pseudo *vic* GTPase-domain gene—HG799051. *C. parasitica* genome sequence reads have been deposited with the National Center for Biotechnology Information Sequence Read Archive under accession no. SRP040304.
[1]Corresponding author: Institute for Bioscience and Biotechnology Research, University of Maryland, 9600 Gudelsky Dr., Rockville, MD 20850. E-mail: dnuss@umd.edu

an incompatible reaction that triggers localized cell death (reviewed by Glass *et al.* 2000; Saupe 2000). This form of conspecific nonself recognition is know as heterokaryon incompatibility or, as used here, vegetative incompatibility, and the corresponding genetic determinants are known as *het* or *vic* loci (Smith and Lafontaine 2013).

While vegetative incompatibility is widespread in filamentous fungi (reviewed in Smith and Lafontaine 2013), the origins and biological functions of these fungal nonself recognition systems remain enigmatic. Two nonexclusive hypotheses have been forwarded (Saupe 2000). The accidental hypothesis proposes that vegetative incompatibility does not have a function but is the result of some evolutionary coincidence that resulted in the formation of polymorphic alleles that are detrimental when combined, *e.g.*, as a result of anastomosis. A prediction of this hypothesis is that the *vic* genes would not be dedicated to allorecognition but would have biological functions in addition to nonself recognition. The allorecognition hypothesis proposes that vegetative incompatibility functions primarily to reduce transmission of deleterious genetic elements such as mycoviruses (Caten 1972), transposable elements (Kinsey 1990), or parasitic nuclei (Debets and Griffiths 1998). A prediction of this hypothesis is that *vic* genes are dedicated to nonself recognition and that dual functions would be rare.

The genetic and molecular characterization of *vic* genes has been limited to three ascomycetes, the model fungi *Neurospora crassa* and *Podospora anserina* and, more recently, the plant pathogenic fungus *Cryphonectria parasitica*, the chestnut blight fungus. Genes have been characterized for 3 of the 11 genetically defined *N. crassa* incompatibility loci and 3 of the 9 *P. anserina* incompatibility loci (reviewed by Smith and Lafontaine 2013). The characterized *vic* genes exhibited high levels of allelic polymorphism as a result of diversifying selection (Hall *et al.* 2010; Bastiaans *et al.* 2014), and several have been shown to have dual functions; *e.g.*, *N. crassa mat-A1* and *mat-a1* genes are involved in transcriptional regulation of mating type (Glass *et al.* 1990; Staben and Yanofsky 1990), *N. crassa un-24* encodes the large subunit of ribonucleotide reductase (Lafontaine and Smith 2012), and *P. anserina* het-C encodes a glycolipid transferase protein (Saupe *et al.* 1994). While diversifying selection of *vic* genes supports the allorecognition hypothesis and dual function of *vic* genes supports the accidental hypothesis, the analyses are limited to a subset of the genetically defined *vic* loci for the two fungi.

Unlike *N. crassa* and *P. anserina*, *C. parasitica* is known to be subjected to widespread infections in nature by a family of viruses, the Hypoviridae, that can reduce ecological fitness, *e.g.*, loss of female fertility, reduced asexual reproduction, and reduced virulence on the plant host (reviewed by Nuss 2005; Dawe and Nuss 2013). Hypovirus-mediated attenuation of *C. parasitica* virulence, termed "transmissible hypovirulence," naturally moderated the chestnut blight epidemic in Europe and provided the basis for applied biological control (Anagnostakis, 1982a, 1983, 1988). Because mycoviruses generally replicate without an extracellular phase, they are transmitted primarily by fungal anastomosis (Ghabrial and Suzuki 2009). The incompatible reaction and accompanying localized cell death triggered by the *vic* system is predicted to constrain cytoplasmic exchange, thus restricting virus transmission.

Genetic studies have defined six *C. parasitica vic* loci with only two alleles at each locus (Anagnostakis 1982b; Huber 1996; Cortesi and Milgroom 1998). Subsequent studies have confirmed that allelic differences at any of the individual *vic* loci, except *vic4*, restrict hypovirus transmission with a magnitude related to the rate at which programmed cell death (PCD) occurs after hyphal fusion (Liu and Milgroom 1996; Cortesi *et al.* 2001; Biella *et al.* 2002). However, it must be noted that, since the heteroallelic strains were not isogenic, it has not been possible to rule out the possibility that non-*vic* genetic determinants contribute to restriction of virus transmission. In the strictest sense, the allorecognition hypothesis would predict that the *C. parasitica vic* genes should be primarily, if not exclusively, dedicated to nonself recognition and that their disruption would allow unrestricted virus transmission without significant negative effects on other biological functions.

Difficulties in identifying *vic* genes have hampered progress in understanding the molecular mechanisms of fungal vegetative incompatibility. Recent efforts to identify fungal *vic* genes based on sequence homology with *N. crassa* and *P. anserina vic* genes have not been fruitful (Fournier *et al.* 2003; Kerenyi *et al.* 2006; Pal *et al.* 2007; Van Diepeningen *et al.* 2008; Iotti *et al.* 2012; Van Der Nest *et al.* 2014). Using a strategy based on polymorphism-guided comparative genomics and on information about *vic* genetic markers, we recently identified seven incompatibility genes associated with four of the six *C. parasitica vic* loci (Choi *et al.* 2012). We now report an extension of this approach to identify the remaining *vic* loci, *vic1* and *vic3*. In addition to polymorphisms in candidate *vic* genes, allelic heterogeneity includes a sequence inversion and a sequence insertion associated with *vic1* as well as a sequence deletion at a nonfunctional pseudo *vic* locus. Functional analysis revealed evidence for both polymorphic and idiomorphic allelic components as well as allelic and nonallelic interactions. These studies formally demonstrate that five of the six *C. parasitica vic* loci contribute to restriction of virus transmission; as noted above, *vic4* was previously shown not to restrict virus transmission. Disruption of 11 *vic* genes associated with the same five *vic* loci resulted in no detectable phenotypic changes in addition to altered incompatibility reactions or virus transmission, which is consistent with a dedicated allorecognition function of the *vic* loci. The molecular identification of the full complement of genetically defined *C. parasitica* loci provides new prospects for manipulation of the *vic* alleles to enhance hypovirus transmission and biological control.

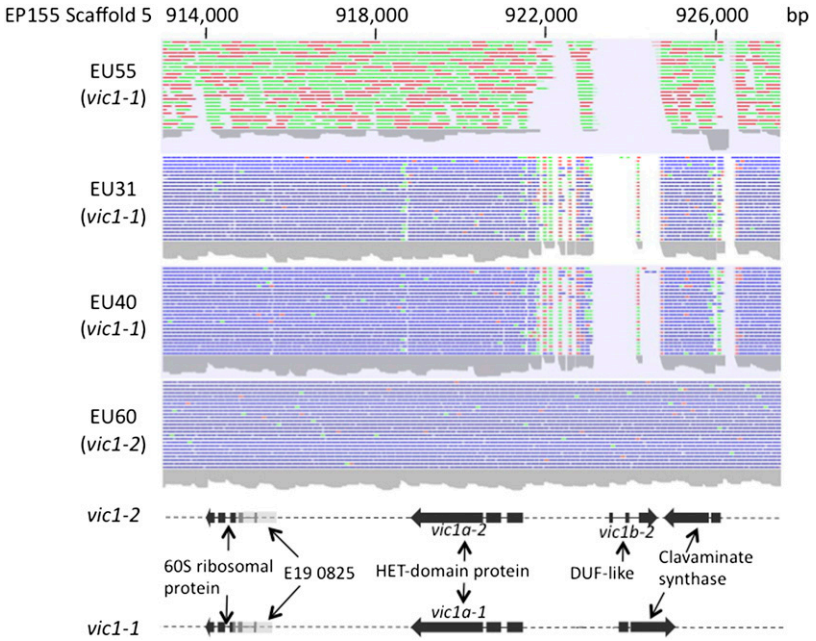

Figure 1 The candidate *vic1* locus. Density plots of sequence reads that match by sequence similarity to a corresponding portion of Scaffold 5 of the EP155 reference genome assembly (coordinates indicated at the top) near a *vic1* linkage marker (E190825) are shown for three strains that differ from EP155 (2211-22) at the *vic1* locus (allele 1), EU55 (1221-22), EU31 (1211-22), and EU40 (1122-11) and for strain EU60 (2221-22) that is the same as EP155 at the *vic1* locus (allele 2). Strain EU55 was sequenced using Roche 454 GS FLX Titanium protocols, and the other strains were sequenced with Illumina HiSeq protocols. Forward reads are indicated in green, reverse reads are indicated in red, paired reads are indicated in blue. The region containing the highly polymorphic sequences is indicated by the absence of matched reads (gap). The ORFs located within a ~14-kb region containing the gap are shown below the sequence read-density plots. A polymorphic gene encoding a HET-domain-containing protein (91% amino acid identity between alleles 1 and 2) was designated as *vic1a-1* for allele 1 present in EU31, EU40, and EU55 and as *vic1a-2* for allele 2 present in reference strain EP155 and strain EU60. The gene encoding the DUF1909-domain-containing protein present in allele 2, but absent in allele 1 (*i.e.*, idiomorphic), was designated *vic1b-2*. The position of the *vic1* linkage marker E190825 relative to the *vic1* gene candidates is also indicated. The *C. parasitica* strain EP155 reference genome assembly is available at http://genome.jgi.doe.gov/Crypa2/Crypa2.home.html. The Joint Genome Institute (JGI) protein identity (ID) numbers for *vic1a-2* and *vic1b-2* are 330677 and 356517, respectively.

Materials and Methods

Fungal strains and growth conditions

C. parasitica strains used in this study included wild-type and genome reference strain EP155 (ATCC 38755) and *vic*-genotyped tester strains (Cortesi and Milgroom 1998) EU31 (ATCC MYA-1074), EU40 (ATCC MYA-1083), EU55 (ATCC MYA-1098), and EU60 (ATCC MYA-1103). *C. parasitica* strain DK80, a mutant of EP155 containing a disruption of the nonhomologous end-joining DNA repair pathway *ku80* gene homolog to promote homologous recombination (Lan *et al.* 2008), was used for most gene disruption analyses. *C. parasitica* field isolates collected from Japan (Liu and Milgroom 2007) and Maryland (Milgroom and Cortesi 1999) were kindly provided by Michael Milgroom (Cornell University). All strains were cultured on potato dextrose agar (PDA) at room temperature on the bench top, unless indicated otherwise.

Genome sequencing and analysis

Genome sequence data and gene model predictions for *C. parasitica* strain EP155 are accessible through the Joint Genome Institute of the U.S. Department of Energy (http://genome.jgi.doe.gov/Crypa2/Crypa2.home.html). Genome sequencing of *C. parasitica vic*-genotyped tester strains EU31, EU40, and EU60 was performed at the University of Maryland DNA sequencing facility according to Illumina HiSeq protocols for generating 100-base paired-end reads. Additionally, strain EU55 DNA was taken through two rounds of sequencing according to the Roche 454 GS FLX Titanium protocols for library preparation, emulsion PCR reaction, and sequencing (Margulies *et al.* 2005). Sequence reads were deposited in the National Center for Biotechnology Information (NCBI) Sequence Read Archive under study accession no. SRP040304. Genomic DNA used for sequencing was prepared after the method of Borges *et al.* (1990). Sequence reads were mapped by similarity to the EP155 reference genome scaffold assemblies with CLC Genomics Workbench 6.0 (CLCBio, Cambridge, MA). Sequence assembly contigs containing candidate *vic* alleles were analyzed with FGENESH (hosted by Softberry at http://linux1.softberry.com) for gene and protein predictions and with NCBI's conserved domain searches (http://www.ncbi.nlm.nih.gov/Structure/cdd/wrpsb.cgi) to identify conserved protein domains in FGENESH-predicted ORFs. The sequences of assembled contigs generated from raw sequence reads for the *vic1* allele of the nonreference strain, *e.g.*, the *vic1-1* allele in strain EU31, was confirmed by DNA sequencing of overlapping PCR amplicons generated from genomic DNA of the corresponding resequenced strains. Protein sequence alignments were performed with MUltiple Sequence Comparison by Log Expectation (MUSCLE at http://www.ebi.ac.uk/Tools/msa/muscle) and alignments visualized in JalView (http://www.jalview.org). The *vic1* alleles were further analyzed by BLAST alignment of the corresponding nucleotide sequences in WebACT (http://www.webact.org/WebACT/home) for visualization of the relative genetic organization at each allele with the Artemis Comparison Tool (ACT) (Sanger Institute, Cambridge, UK).

GenBank accession numbers for the candidate *vic* genes are as follows: *vic1a-1*, HG799041; *vic1a-2*, HG799042; *vic1b-2*,

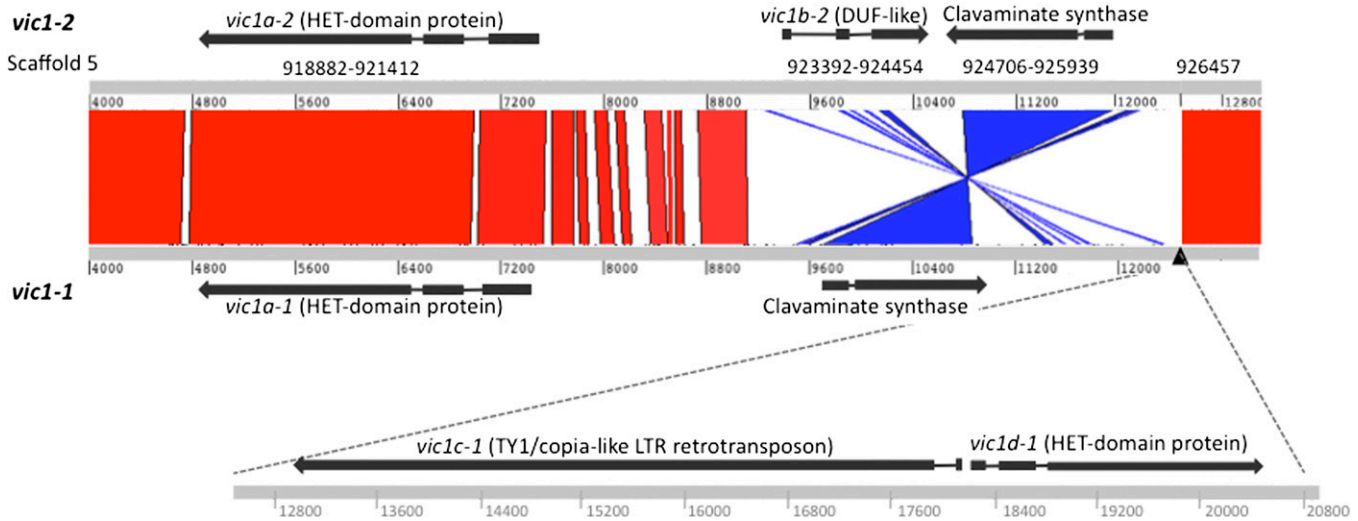

Figure 2 Comparison of the gene order at the *vic1-1* and *vic1-2* alleles. The sequences at the two alleles were BLAST-aligned in WebACT (http://www.webact.org/WebACT/home) for visualization of the genetic organization at each allele relative to that at the other with the Artemis Comparison Tool. High-scoring alignments are visualized in red (forward matches) and blue (reverse matches); the cutoff for an alignment was set at an ID score of ≥16. The *vic1* locus contains a region that has undergone a sequence inversion affecting the orientation of a putative clavaminate synthatase-like gene relative to that of the predicted HET gene. Allele 1 is indicated below the alignment drawn to approximate scale. Note that allele 1 also contains a ~8.5-kb insertion that is absent in allele 2. The allele-1-specific sequence contained two ORFs encoding a 689-aa HET-domain-containing protein (designated *vic1d-1*) and a 1619-aa TY1/copia-like LTR retrotransposon (designated *vic1c-1*) as indicated below the allele sequence alignment.

HG799043; *vic1c-1*, HG799048; *vic1d-1*, HG799049; *vic3a-1*, HG799044; *vic3a-2*, HG799045; *vic3b-1*, HG799046; *vic3b-2*, HG799047; pseudo *vic* HET-domain gene, HG799050; and pseudo *vic* GTPase-domain gene, HG799051.

Disruption of candidate vic genes

Disruption of candidate *vic* genes was performed by homologous recombination in *C. parasitica* strain DK80 using PCR-generated disruption fragments based on the strategy of Kuwayama *et al.* (2002) with modifications as described by Zhang *et al.* (2013). Disruption of both *vic* candidate genes *vic3a-2* and *vic3b-2* was also accomplished in strain EU60. DNA-mediated transformation was performed according to the method of Churchill *et al.* (1990), followed by selection of putative transformants grown in the presence of 40 μg/ml hygromycin B or 25 μg/ml G418 for neomycin-resistance selection. Gene disruption was confirmed by PCR analysis of the putative transformants, followed by selection of uninuclear single conidial isolates on antibiotic-containing PDA to eliminate heterokaryons and by a final PCR confirmation. Conditions used for PCR were as described in Zhang *et al.* (2013) on fungal DNA extracted according to Spiering *et al.* (2008).

Analysis of fungal phenotype, mycelial incompatibility, and virus transmission

Colony morphology, asexual conidia production, and fungal virulence were assessed according to standard procedures (Hillman *et al.* 1990). Mycelial incompatibility and virus transmission assays were performed as described in Choi *et al.* (2012). Hypovirus CHV-1/EP713 infection was established in the different *vic*-genotyped tester strains, strain DK80, and *vic1* and *vic3* disruption strains by transfecting fungal spheroplasts with CHV-1/EP713 transcripts generated *in vitro* from a full-length viral complementary DNA as described by Chen *et al.* (1994).

Results

Polymorphism-based identification of the C. parasitica vic1 and vic3 loci

The polymorphism-based comparative genomics approach used for molecular identification of *vic2*, *vic4*, *vic6*, and *vic7* (Choi *et al.* 2012) was extended here to identify the *vic1* and *vic3* loci. Genotyped *vic* tester strains (Cortesi and Milgroom 1998) that differed from the reference strain EP155 at *vic1* and/or *vic3* were resequenced by high-throughput sequencing protocols. The convention for *vic* genotypes specifies which allele, designated 1 or 2, is present at the individual *vic* genetic loci; *e.g.*, the EP155 *vic* genotype is *vic1-2*, *vic2-2*, *vic3-1*, *vic4-1*, *vic6-2*, and *vic7-2* (abbreviated to 2211-22). Raw sequence reads were mapped to the EP155 reference genome assembly by sequence similarity, and regions of significant hypervariability, appearing as gaps in the sequence read-density plots, were identified. Molecular markers linked to the *vic1* locus were used as guides to locate *vic1* candidate polymorphic regions. The absence of *vic3*-specific molecular linkage markers required the use of manual inspection to identify polymorphic *vic3* candidates. The resequenced strains included EU-31 (1211-22), which differs from the reference strain EP155 (2211-22) at the *vic1* locus;

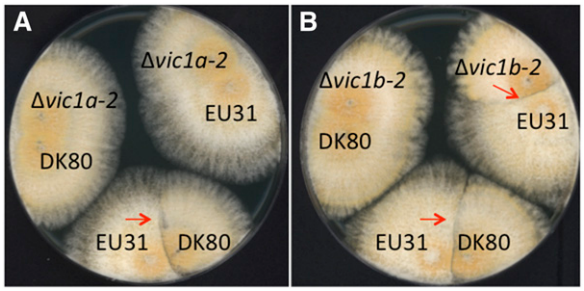

Figure 3 Mycelial incompatibility assay for strains disrupted in candidate *vic* alleles *vic1a* and *vic1b* in strain DK80 (2211-22) (barrage lines indicated by red arrows). (A) Barrage formation resulting from an incompatible reaction occurred when strain DK80 (2211-22) was paired with strain EU31 (1211-22), but was abolished when DK80 *vic1a-2*-disrupted strain Δ*vic1a-2* (⇄2211-22) was paired with strain EU31 (1211-22). (B) Barrage formation was retained, but was less pronounced, when DK80 *vic1b-2*-disrupted strain Δ*vic1b-2* (⇄2211-22) was paired with tester strain EU31 (1211-22).

Table 1 Hypovirus transmission frequency for disruption mutants of candidate *vic1* alleles

Donor	Recipient	Transmission	Note
DK80 (2211-22)	EP155 (2211-22)	20/20	
EP155 (2211-22)	DK80 (2211-22)	20/20	
DK80 (2211-22)	EU31 (1211-22)	20/20	PDA
DK80 Δ*vic1a-2* (⇄2211-22)	EU31 (1211-22)	20/20	Medium
EU31 (1211-22)	DK80 (2211-22)	2/20	
EU31 (1211-22)	DK80 Δ*vic1a-2* (⇄2211-22)	20/20	
DK80 (2211-22)	EP155 (2211-22)	20/20	
EP155 (2211-22)	DK80 (2211-22)	20/20	
DK80 (2211-22)	EU31 (1211-22)	20/20	GBR
DK80 Δ*vic1b-2* (⇄2211-22)	EU31 (1211-22)	20/20	Medium
EU31 (1211-22)	DK80 (2211-22)	6/20	
EU31 (1211-22)	DK80 Δ*vic1b-2* (⇄2211-22)	20/20	

GBR: PDA supplemented with 7 g/liter malt extract, 2 g/liter yeast extract, 0.8 g/liter tannic acid, 50 mg/ liter Bromocresol Green, 20 g/liter additional agar, and 12 drops/liter of Tween 20) (modified from Powell 1995).

EU-60 (2221-22), which differs from EP155 at the *vic3* locus; EU-55 (1221-22), which differs from EP155 at both the *vic1* and *vic3* loci; and EU-40 (1122-11), which differs from EP155 at all six genetically identified *vic* loci. Illumina HiSequation 1000 protocols for generating 100-base paired-end reads were used for strains EU-31, EU-40, and EU-60. Strain EU-55 DNA was sequenced using Roche 454 GS FLX Titanium protocols. More than 15 million reads for each of the EU strains were mapped to the EP155 reference sequence using CLC Genomics Workbench.

Identification of the candidate vic1 locus

Inspection of the EU-31 (1211-22; *vic1*, allele 1) reads mapped to EP155 (2211-22; *vic1*, allele 2) Scaffold 5 in a region that contained *vic1* linkage markers (Supporting Information, Figure S1) resulted in the identification of a gap in the read-density plot (Scaffold 5: 921500–926500), suggesting polymorphism located ~6 kb from the linkage marker E19 0825 (Figure 1). A similar gap was observed in the density plots for EU55 and EU40, which also contained the *vic1-1* allele, but not for EU60, which contained the *vic1-2* allele also present in reference strain EP155. This polymorphic region in strain EP155 consisted of an ORF encoding a 771-amino-acid-long protein containing an heterokaryon or HET domain (Pfam: PF06985) (Smith *et al.* 2000), conserved in genes found in the three characterized *vic* loci in *N. crassa* and two of the three characterized *vic* loci in *P. anserina* (reviewed in Smith and Lafontaine 2013) and an adjacent ORF that encodes a 172-amino-acid-long hypothetical protein containing a DUF1909 (conserved domain of unknown function) domain. The ORF encoding the HET-domain protein in strains EP155 and EU60 was designated *vic1a*-allele 2 (*vic1a-2*), and the corresponding ORF in strains EU31, EU40, and EU55 was designated *vic1a*-allele 1 (*vic1a-1*). The corresponding *vic1a-1* and *vic1a-2* HET proteins showed 91% identity at the amino acid level (Figure S2). This level of sequence heterogeneity was lower than that observed for the other *C. parasitica vic* genes [*e.g.*, the HET-domain-containing *vic6* alleles show 53% overall amino acid identity (Choi *et al.* 2012)]. The ORF encoding the DUF1909-domain protein in strain EP155 was designated *vic1b-2*. Interestingly, *vic1b-2* in strain EP155 is idiomorphic rather than polymorphic. That is, the *vic1b-2* sequence is absent in the corresponding *vic1-1* region.

Further analysis and confirmation of the nucleotide sequence assembly contigs spanning the entire *vic1-1* allele by sequencing of overlapping PCR amplicons generated from EU31 and EU55 genomic DNAs revealed evidence of a sequence inversion and a sequence insertion in *vic1-1* relative to the *vic1-2* sequence. A conserved ORF encoding a clavaminate synthase-like protein (Figure S3) was found to be in opposite orientation in *vic1-1* and *vic1-2* relative to the orientation of the predicted HET-domain genes. Interestingly, an insertion of ~8.5 kb that contained two ORFs encoding a 1619-aa-long TY1/copia-like LTR retrotransposon (designated *vic1c-1*) and an adjacent 689-aa-long HET-domain protein (designated *vic1d-1*) was found next to the inverted clavaminate synthase-like gene in *vic1-1*. The relative genetic organization of the two alleles is shown in Figure 2, visualized as a BLAST alignment of the *vic1-1* and *vic1-2* nucleotide sequences in the Artemis Comparison Tool (available at WebACT at http://www.webact.org/WebACT/home) with a depiction of the *vic1-1* sequence insert drawn to approximate scale.

Disruption and functional analysis of the candidate vic1-2 genes

Where colonies of two *vic* incompatible *C. parasitica* strains come into contact, a zone of demarcation (called a "barrage") forms, which is composed of lysed and dead cells (Powell 1995). Barrage formation is considered a form of mycelial incompatibility (Smith *et al.* 2006), and the incompatibility reaction is described as having the hallmarks of PCD (Biella *et al.* 2002 and reviewed in Smith and Lafontaine 2013).

The candidate genes at allele 2 of the *vic1* locus, *vic1a*-2 and *vic1b-2*, were independently disrupted in the DK80

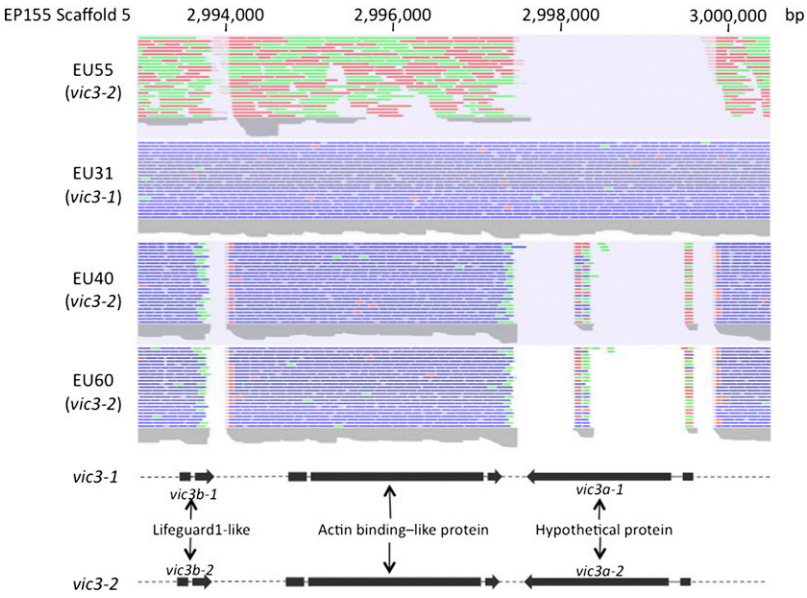

Figure 4 The candidate *vic3* locus. Read-density plots of sequence reads mapped by homology to a ~7.5-kb portion of Scaffold 5 of the EP155 reference genome assembly identified by manual inspection to contain a region of sequence polymorphism (gaps) with a pattern consistent with that for allele distributions at the *vic3* locus. Density plots are shown for strains EU55 (1221-22), EU40 (1122-11), and EU60 (2221-22) that differ at the *vic3* genetic locus (*i.e.*, contain allele 2) from reference strain EP155 (2211-22) and strain EU31 (1211-22) that, like strain EP155, contains allele 1 at the *vic3* locus (Cortesi and Milgroom 1998). The ORFs located within this region are shown for the two alleles below the sequence read-density plots. Polymorphic (46% amino acid identity) ORFs encoding a hypothetical protein were designated *vic3a-1* (599 aa) for allele 1 in strains EP155 and EU31 and *vic3a-2* (614 aa) for allele 2 present in strains EU55, EU40, and EU60, while two small polymorphic (85% amino acid identity) ORFs encoding a Life-guard-1-like protein were designated *vic3b-1* (102 aa) and *vic3b-2* (108 aa). These two polymorphic genes were separated by a highly conserved ORF encoding an actin-binding-like protein. Sequencing protocols and color coding of reads are described in Figure 1. The JGI protein ID numbers for *vic3a-1* and *vic3b-1* are 331201 and 340400, respectively. The protein ID number for the predicted actin-binding-like protein is 331200.

nonhomologous end-joining mutant strain of EP155 as described in Figure S4. While strains DK80 and EU-31 underwent an incompatible reaction, clearly forming a barrage when paired, the Δ*vic1a-2* disruption mutant was compatible with EU-31 (Figure 3A). Thus, disruption of the *vic1a* allele in just one of the paired *vic1* heteroallelic strains resulted in loss of barrage formation.

The influence of heteroallelism at the *vic1* locus on virus transmission is highly asymmetric (Cortesi *et al.* 2001). No resistance to virus transmission is observed if the recipient strain contains allele 1, while transmission is only ~10% if the recipient strain contains allele 2. As indicated in Table 1, deletion of the *vic1a-2* allele resulted in an increase in virus transmission from ~10 to 100% in pairings in which the mutant strain served as the virus recipient and strain EU-31 served as the virus donor. The combined loss of barrage formation and increased virus transmission observed for the Δ*vic1a-2* mutant strain, coupled with the concordance between the allele nucleotide sequence specificity and *vic* genotypes for EP155, EU55, EU31, EU40, and EU60 (Figure 1), provide strong evidence that the *vic1a-2* gene is a functional component of the *vic1*-locus.

Disruption of the *vic1b-2* allele (Figure S4) resulted in reduced growth and altered morphology (Figure S5). This altered phenotype complicated the interpretation of barrage formation and virus transmission experiments. However, the growth and morphology alterations were ameliorated when the mutants were grown on enriched medium (Figure S5). Under these conditions, when paired with strain EU31, the Δ*vic1b-2* mutant strain showed reduced, but not loss of, barrage formation (Figure 3B) and increased virus transmission from 20–30% to 100% when serving as the recipient (Table 1). These combined results demonstrate that the *vic1b-2* ORF also contributes to the *vic-1*-associated incompatible reaction.

Interestingly, the Δ*vic1b-2* slow-growth phenotype was more severe when the fungus was grown in the dark, while the growth difference between the Δ*vic1b-2* and DK80 strains was less pronounced when both strains were infected with hypovirus CHV-1/EP713 (Figure S5). Although the Δ*vic1b-2* mutant exhibited a reduced growth rate, asexual sporulation per unit of mycelial mass was several fold higher than that of the parental strain under standard culture conditions (data not shown). Consistent with the slower growth in culture, the Δ*vic1b-2* mutant strain formed cankers on dormant chestnut stems that were ~35% smaller than those formed by strain DK80, *i.e.*, demonstrated a moderate level of reduced virulence (data not shown). These phenotypic changes were observed for multiple independent *vic1b-2*-disruption mutants. Extended sequence analysis of two of these independent disruption mutants showed no unintended sequence modifications extending upstream into *vic1a-2* and downstream through the entire clavaminate synthase gene (results not shown). Note that *vic1b-2* is the only *C. parasitica* candidate *vic* gene for which a phenotypic change has been observed upon disruption.

Identification of the candidate vic3 locus

Since the parental strains used to generate the *C. parasitica* linkage map (Kubisiak and Milgroom 2006) were homoallelic at *vic3*, no molecular linkage marker sequences were available to serve as guides to the location of the *vic3* locus. Consequently, the sequence read-density plots were examined manually for gaps that occurred when reads from *vic3-2* allelic strains EU55 (1221-22), EU40 (1122-11), and EU60

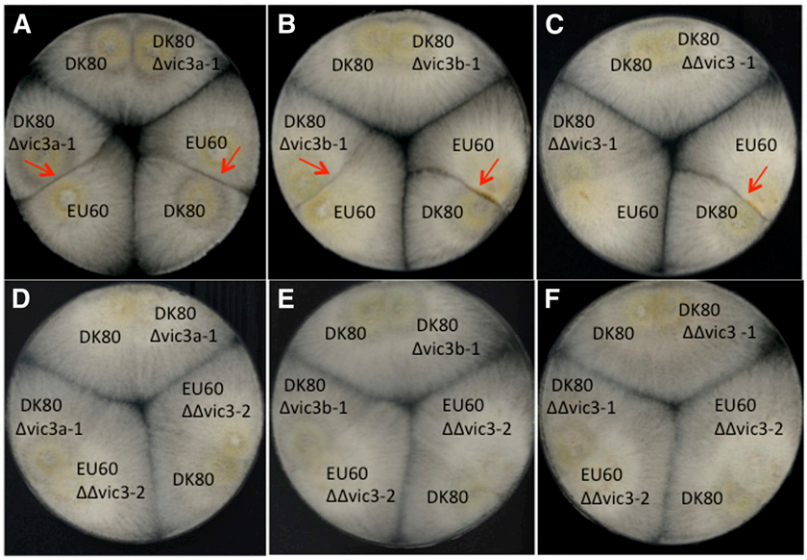

Figure 5 Mycelial incompatibility assay for strains disrupted in candidate *vic* alleles *vic3a* and *vic3b* in the incompatible strains DK80 (2211-22) and EU60 (2221-22). Barrage formation resulting from an incompatible reaction occurred when *vic3a* mutant DK80 Δ*vic3a-1* (2211-22) was paired with tester strain EU60 (2221-22) (A) and when *vic3b* mutant DK80 Δ*vic3b-1* (2211-22) was paired with EU60 (2221-22) (B) (barrage lines indicated by red arrows). In contrast, barrage formation was abolished when double *vic3a-1/vic3b-1* mutant strain DK80 ΔΔ*vic3-1* (2211-22) was paired with EU60 (2221-22) (C). Barrage formation was also abolished for the reciprocal pairing involving the EU60 double *vic3a-2/vic3b-2* mutant strain EU60 ΔΔ*vic3-2* (2221-22) and DK80 (2211-22) (D). As expected, no barrage formed when the EU60 ΔΔ*vic3-2* (2221-22) mutant strain was paired with either of the DK80 ΔΔ*vic3-1* (2211-22) double-mutant strain (F) or the DK80 Δ*vic3a-1* (2211-22) or DK80 Δ*vic3b-1* (2211-22) single-mutant strains (D and E, respectively).

(2221-22) were mapped to the *vic3-1*-containing EP155 (2211-22) genome sequence, but that were absent in the plot for strain EU31 (1211-22), which also contains the *vic3-1* allele.

A 7-kb-long span containing two such gaps was identified on Scaffold 5 ~2 Mb away from the *vic1* locus at map position 2,993,000–3,000,000 (Figure 4). Gap 1 was 2.4 kb in size and included the coding sequence for a hypothetical protein consisting of 599 and 614 amino acids in *vic3-1* and *vic3-2*, respectively, designated *vic3a-1* and *vic3a-2*. With only 46% identity between *vic3a-1* and *vic3a-2*, this protein displayed significant allelic sequence divergence (Figure S6). Gap 2 consisted of a short ~200-bp-long region located 3.4 kb away from gap 1 and contained the 3′-terminal end of an ORF for a short glycine–glutamine-rich protein of 102 and 108 amino acids in *vic3-1* and *vic3-2*, respectively, designated *vic3b-1* and *vic3b-2*. The predicted *vic3b* proteins had significant (*e*-value <1*e*-05) similarity to glutamate-receptor-associated, Lifeguard-1-like proteins. The predicted *vic3b-2* protein also contained a 2Fe-2S ferredoxin-type iron-sulfur-binding region signature (PS00197), absent in the *vic3b-1* protein, and the two allelic proteins displayed moderately high similarity (85% identity) (Figure S7). The two polymorphic ORFs were separated by a highly conserved ORF encoding an actin-binding-like protein (Figure 4).

Disruption and functional analysis of the candidate vic3 genes

Similar to the strategy used for disruption of *vic1a-2* and *vic1b-2*, the *vic3* candidate genes *vic3a-1* and *vic3b-1* in strain DK80 were independently disrupted as described in Figure S8A. Unlike the observation for the *vic1a-2* disruption mutant, the individual Δ*vic3a-1* and Δ*vic3b-1* mutant strains retained the ability to form a barrage when paired with the *vic3* heteroallelic strain EU60 (2221-22) (Figure 5, A and B). Consequently, deletion of both *vic3a* and *vic3b* ORFs was undertaken. A double *vic3a-1/vic3b-1* mutant in strain DK80 (2211-22) was generated by disrupting *vic3b-1* in the existing *vic3a-1* mutant, leaving the actin-binding-like gene intact (Figure S8A). A *vic3-2* double mutant was also generated by disrupting *vic3a-2*, *vic3b-2*, and the intervening actin-binding-like gene in strain EU60 (2221-22), as described in Figure S8B. Barrage formation was eliminated when the DK80 Δ*vic3a-1/*Δ*vic3b-1* double-mutant strain was paired with EU60 (2221-22) and when the EU60 Δ*vic3a-2/*Δ*vic3b-2* double mutant was paired with DK80 (2211-22) (Figure 5, C and D). As expected, no barrage formed when either of the double-mutant strains was paired with the heteroallelic mutant strain deleted for *vic3a* or *vic3b* (Figure 5, D–F).

The effect of *vic3* component genes on hypovirus transmission was somewhat complicated as indicated in Figure 6. As shown in Figure 6, heteroallism at the *vic3* locus for DK80 (2211-22) and EU60 (2221-22) resulted in a significant resistance to hypovirus transmission: 10–17% of pairings resulted in virus transmission no matter which strain was the donor or the recipient. Disruption of the *vic3a-1* gene in DK80 resulted in 100% virus transmission, but only when the mutant strain served as the recipient. In contrast, disruption of the *vic3b-1* gene in DK80 resulted in 100% transmission, but only if the mutant strain served as the donor. Similar to previous observations for the *vic6* locus (Choi *et al.* 2012), these asymmetric increases in virus transmission occurred even though barrage formation was still observed. As expected, disruption of both *vic3a* and *vic3b* in DK80 completely removed resistance to virus transmission in both directions when paired with strain EU60. Similarly, virus transmission was 100% in both directions when an EU60 strain containing disruptions of both *vic3a-2* and *vic3b-2* was paired with strain DK80. These results clearly demonstrate that the *vic3a* and *vic3b* genes are functional components of the *vic3* locus.

Curiously, virus transmission remained slightly restricted between DK80 containing the Δ*vic3b-1* disruption and EU60 containing the *vic3a-2* + *vic3b-2* double disruption (45/60) only when the DK80 *vic3b-1* mutant was the donor and

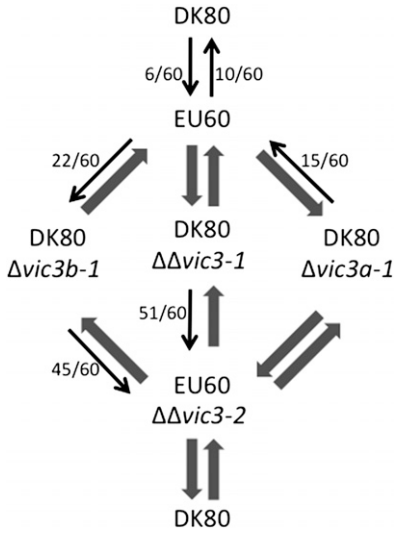

Figure 6 The effect of *vic3* locus mutations on hypovirus transmission. Pairing of *vic3* heteroallelic strains DK80 (2211-22) and EU60 (2221-22), indicated at the top, resulted in a significant and symmetrical restriction in virus transmission: only 10–17% of pairings resulted in hypovirus transmission independent of which strain served as virus donor. The arrows indicate direction of virus transmission, with thin arrows indicating a level of restriction shown in parentheses and thick arrows indicating 100% (60/60) transmission. Virus transmission increased to 100% when *vic3a-1* was disrupted in strain DK80 (DK80Δ*vic3a-1*) and paired with EU60, if the mutant strain served as the recipient, and increased only slightly (from 10/60 to 15/60) if the mutant served as the donor. Disruption of *vic3b-1* in DK80 (DK80Δ*vic3b-1*) also increased virus transmission to 100%, but only when the mutant strain served as the donor, and increased from 6/60 to 22/60 when the mutant served as the recipient. Virus transmission increased to 100% in both directions when both *vic3a-1* and *vic3b-1* in DK80 were disrupted (DK80ΔΔ*vic3-1*) and paired with EU60. Unexpectedly, virus transmission remained slightly restricted when the DK80 ΔΔ*vic3-1* and EU60 ΔΔ*vic3-2* double-mutant strains were paired, but only when the DK80 mutant strain was the donor. An unexpected slight restriction was also observed when the DK80 Δ*vic3b-1* mutant was paired as donor with the EU60 ΔΔ*vic3-2* double-mutant strain. No restriction was observed when DK80 or DK80Δ*vic3a-1* was paired with the EU60 ΔΔ*vic3-2* double mutant, similar to the observation for pairing of EU60 with the DK80ΔΔ*vic3-1* double mutant.

between the EU60 double and the DK80 double *vic3a* + *vic3b* disruption mutants when the DK80 double mutant was the donor (51/60). Additional in-depth studies of *vic3* component gene interactions will be required to understand the basis of this residual resistance, *e.g.*, the possible influence of eliminating the actin-binding-like gene in the EU60 *vic3* double mutant.

Polymorphism-based identification of a nonfunctional pseudo vic locus containing a HET-domain gene deletion

The manual inspection of the sequence read-density plots conducted during the search for *vic3*-related polymorphic regions identified an additional polymorphic region that contained genes similar to those found at other *vic* loci. Located on Scaffold 6, spanning region 599514-606808 (Figure 7), the gap was found for strains EU31, EU55, and EU60, but not for strain EU40. Two ORFs were identified at this position in the EP155 sequence assembly, arbitrarily designated allele 1, that encoded a 1211-aa HET-domain protein and a 407-aa protein with a GTPase domain (Figure 8). Interestingly, there was no correspondence between the pattern of allele specificity at this position and the pattern of allele distributions at the genetically defined *vic* loci for the resequenced strains. For example, EP155 (2211-22) and EU40 (1122-11) are heteroallelic at all six genetically defined *vic* loci, but are homoallelic at this locus.

Inspection of sequence contigs for the allele present in EU31, EU55, and EU60, designated allele 2, indicated that the polymorphism was due to the absence of the GTPase and HET-domain ORFs and flanking noncoding regions as shown in Figure 8. Note the presence of ~900-bp direct repeats of 88% identity flanking the polymorphic region in allele 1 and the presence of a single chimeric repeat in the corresponding allele 2. Close inspection showed that the remaining single copy of the repeat sequence present in allele 2 is chimeric with two-thirds of the sequence coming from the left-flanking repeat and one-third from the right-flanking repeat (Figure S9). The chimeric nature of the remaining repeat sequence is consistent with deletion of the region containing the HET-domain gene and the GTPase gene by a homologous recombination event.

Indirect evidence indicated that this locus does not currently function in the *vic* nonself recognition system. Barrage formation between EU31 (1211-22) and DK80 (2211-22) was eliminated (Figure 3) by disruption of the *vic1a-2* allele, and unrestricted virus transmission was observed (Table 1) even though, as shown in Figure 7, the DK80/Δ*vic1a-2* mutant and EU31 are heteroallelic at the polymorphic Scaffold 6 locus. However, the possibility that another incompatible allelic form of this locus is present in some *C. parasitica* population cannot be ruled out.

It was of interest to determine whether the HET-domain gene deletion (in allele 2) associated with this nonfunctional locus was more widely distributed in the *C. parasitica* population. Four primer pairs (Table S1) were designed to test for the presence/absence of the left repeat, GTPase gene, HET-domain gene, and chimeric repeat. As shown in Table 2, allele 2 was found in 4 of 14 field isolates obtained from a North American population in Finzel, Maryland (Milgroom and Cortesi 1999), and in 2 of 4 field isolates sampled from an Asian population from Iwama, Ibaraki Prefecture, Japan (Liu and Milgroom 2007). The presence of only alleles 1 and 2 in both North American and Asian *C. parasitica* populations indicates that the deletion at this locus was not a recent event.

Discussion

Interest in the *vic* nonself recognition system operating in *C. parasitica* derives primarily from reports that it restricts transmission of viruses that mediate biological control of chestnut blight (Van Alfen *et al.* 1975; Anagnostakis 1982a; Macdonald and Fulbright 1991; Nuss 1992; Heiniger and Rigling 1994; Milgroom and Cortesi 2004). A major

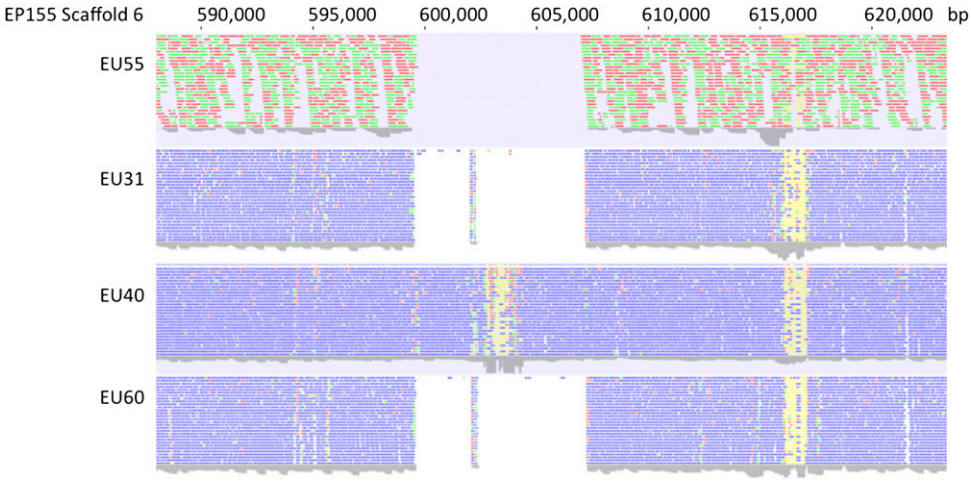

Figure 7 Polymorphic nonfunctional pseudo *vic* locus. Density plots of sequence reads mapped by homology to a portion of EP155 (2211-22) sequence assembly Scaffold 6 extending from map coordinates ~588,000 to 624,000 are shown for strains EU55 (1221-22), EU31 (1211-22), EU40 (1122-11), and EU60 (2221-22). The defined gap observed at 599,514–606,808 for strains EU55, EU31, and EU60 relative to EP155 and EU40 corresponds to allelic differences in genome organization at this locus as shown in Figure 8 for allele 1 (in strains EP155 and EU40) and allele 2 (in strains EU55, EU31, and EU60). There is no concordance between the polymorphic pattern and allele specificity at any of the genetically defined *vic* loci; *e.g.*, EP155 (2211-22) and EU40 (1122-11) are heteroallelic at all six genetically defined *vic* loci, but are homoallelic at this locus.

advancement in understanding the genetic structure of this system came from analyses by Cortesi and Milgroom (1998) that identified six di-allelic loci controlling *vic* in European *C. parasitica* populations and provided a collection of 64 vic tester strains with defined genotypes corresponding to all combinations of the *vic* alleles. The ability to define the *vic* genotype of *C. parasitica* field isolates and laboratory strains has enabled more precise examinations of the relationship between *vic* diversity and virus transmission and the influence of different *vic* loci on virus transmission, leading to the identification of allele-specific influences on the frequency and symmetry of virus transmission (Huber and Fulbright 1994; Cortesi *et al.* 2001; Biella *et al.* 2002). The molecular identification of the *vic1* and *vic3* loci described here, along with the report by Choi *et al.* (2012), completes the molecular identification of all six genetically defined *C. parasitica vic* loci. The identification of the gene compositions of the respective *vic* loci has allowed gene disruption analysis to definitively demonstrate that *vic* genes contribute to restriction of mycovirus transmission and to test whether they have biological functions in addition to allorecognition. This information will also enable more precise population genetic studies, create opportunities to determine molecular mechanisms underlying *vic*-mediated triggering of PCD, and provide the means for manipulating the *vic* system to enhance the transmission and utility of hypoviruses for biological control.

The gene organization and composition uncovered for the *vic1* and *vic3* loci extend the overall level of diversity observed for the *C. parasitica vic* loci. The composition of the *vic1-2* allele is unusual in that it contains the combination of a polymorphic HET-domain gene (*vic1a-2*) and an idiomorphic DUF1909-domain gene (*vic1b-2*). Polymorphic HET-domain genes were also found at the *vic6* and *vic7* loci. However, the association of HET-domain proteins with only three of the six genetically defined *C. parasitica vic* loci contrasts with the observations in *N. crassa*, where all three of the characterized *het* (*vic* equivalent) complexes involve a HET-domain gene, and *P. anserina*, where HET-domain genes are associated with two of the three characterized *het* loci (reviewed in Smith and Lafontaine 2013).

While the *vic1b-2* gene does not have a corresponding polymorphic ORF present in the *vic1-1* allele, remnants of the *vic1b-2* sequence are evident in *vic1-1* and are associated with the sequence inversion that includes the clavaminate synthase-like gene, as indicated by the alignment highlighted in blue shown in Figure 2. This differs from the previously described *vic4* idiomorphs (Choi *et al.* 2012), where a protein kinase c-like gene present in *vic4-1* is replaced with a completely unrelated NACHT-NTP/WD repeat-encoding gene in *vic4-2*. In this regard, the *vic1-1* idiomorph does contain an LTR retrotransposon (*vic1c-1*) and a HET-domain protein gene (*vic1d-1*) that are completely absent in *vic1-2*. *vic1* and *vic4* therefore join the *N. crassa mat-A1/mat-a1/tol* locus (Glass *et al.* 1988) as fungal allorecognition loci involving idiomorphic alleles. The *vic1b-2* and *vic1d-1* sequences are unique and were not found elsewhere in the *C. parasitica* reference genome sequence. However, transposon-like sequences, some having similarity to *vic1c-1*, are common, and their distribution in the genomes of different *C. parasitica* strains is currently under investigation.

Disruption analysis of *vic1-2* genes uncovered additional differences with the other *C. parasitica vic* loci. Disruption of the HET-domain gene *vic1a-2* resulted in elimination of barrage formation and in unrestricted virus transmission when the disrupted strain was paired with one that was heteroallelic at *vic1* (Figure 3). This contrasts with the results for *vic2-2*, *vic6-2*, and *vic7-2* where disruption of their HET-domain genes increased virus transmission but did not eliminate barrage formation (Choi *et al.* 2012). In the case of *vic6*, nonallelic interactions between the *vic6* gene and the adjacent *pix6* gene triggered PCD (Choi *et al.* 2012). The

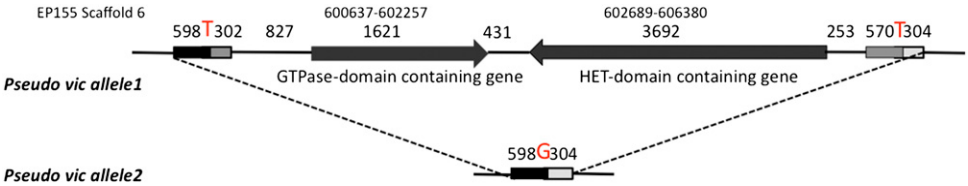

Figure 8 Organization of polymorphic nonfunctional pseudo *vic* locus alleles. Inspection of the sequence contigs for the two alleles corresponding to the polymorphic region identified on Scaffold 6 spanning positions 599514–606808 in the EP155 reference genome assembly revealed that an ~7.7-kb portion of the sequence present in EP155 and EU40 (allele 1) was deleted in strains EU55, EU31, and EU60 (allele 2). The allele 1 sequence contained two ORFs not present in allele 2. These encoded a 407-aa protein containing a GTPase domain and a 1211-aa-long HET-domain-containing protein. The two ORFs were flanked by ~900-bp imperfect (88% identity) direct repeats. The allele 2 sequence lacked the ~7.7-kb region harboring the GTPase and HET-domain ORFs and contained only one copy of the flanking repeats that consisted of the 5′-proximal two-thirds of the left repeat and the 3′-proximal one-third of the right repeat and a G-C base pair replacing a T-A base pair at the breakpoint as indicated by the red letters. (Figure S9).

observation that disruption of the *vic1a* allele in just one of the paired *vic1* heteroallelic strains resulted in loss of barrage formation suggests that an allelic interaction between *vic1a-1* and *vic1a-2* is sufficient to trigger PCD, although *vic1a-1* disruption is required for confirmation.

In contrast to the result of *vic1a-2* disruption, *vic1b-2* disruption failed to eliminate barrage formation. However, as was observed previously for disruption of *vic2-2*, *vic6-2*, and *vic7-2* (Choi *et al.* 2012), disruption of *vic1b-2* increased virus transmission without elimination of barrage formation, presumably due to a slower onset of PCD (Table 1). These results suggest that the *vic1b-2* product is involved in a nonallelic interaction to trigger PCD. The *vic1-1* allele remains to be functionally characterized, and the product of the HET-domain gene *vic1d-1* certainly provides a potential candidate for that interaction. It will also be of interest to determine whether disruption of the LTR-retrotransposon gene, *vic1c-1*, affects nonself recognition or the fungal phenotype.

The *vic3* locus contains two polymorphic genes that are unrelated to any previously identified *C. parasitica vic* genes. The *vic3a* gene products are highly polymorphic (~46% identical) and lack recognizable conserved sequence domains. The *vic3b* gene products are much less polymorphic, but are distinctive in the unusually high level of glycine and glutamine repeats. Since both *vic3a* and *vic3b* alleles must be deleted to eliminate barrage formation, it is likely, but not confirmed, that allelic interactions are insufficient to trigger PCD.

As reported for the nonallelic interactions observed for the *vic6* locus (Choi *et al.* 2012), disruption of *vic3a-1* and *vic3b-1* independently caused an asymmetric change in virus transmission without eliminating barrage formation: the Δ*vic3a-1* disruption mutant became a good recipient, while the Δ*vic3b-1* mutant became a good virus donor (Figure 6). Notably, the virus transmission rates of ~10–17% observed in this study for pairing of the *vic3* heteroallelic strains DK80 (2211-22) and EU60 (2221-22) (Figure 6) differ significantly from the rates of 60–80% reported by Cortesi *et al.* (2001) for other paired *vic3* heteroallelic strains. Virus transmission rates were in excellent agreement in these different studies for paired strains that are heteroallelic at each of the other five *vic* loci. It should be noted that the specific *vic* genotypes of the *vic3*-heteroallelic paired strains used in the Cortesi *et al.* (2001) study did not include the DK80 (2211-22) *vs.* EU60 (2221-22) genotypes used in this study. Irrespective of these transmission rate differences, the results of the *vic3* gene disruption analysis for DK80 and EU60 confirm that *vic3a* and *vic3b* alleles contribute to restriction of virus transmission.

Combined, Choi *et al.* (2012) and this study have identified and characterized 8 polymorphic genes and 5 idiomorphic genes associated with 6 *C. parasitica vic* loci (Table 3). This compares with 5 polymorphic and 2 idiomorpic genes characterized at 3 incompatibility loci in *N. crassa* and 5 genes characterized at 3 loci in *P. anserina* (reviewed in Smith and Lafontaine 2013). Thus, with this recent work on the *C. parasitica* system, the number of fungal allorecognition-associated genes identified at the molecular level has more than doubled. A total of 11 polymorphic and 1 idiomorphic *C. parasitica vic* genes have been disrupted. One potential allelic interaction was detected with the loss of barrage formation upon disruption of *vic1a-2* (Figure 3). Nonallelic interactions were demonstrated for the *vic6* and *pix6* alleles (Choi *et al.* 2012). Nonallelic interactions were inferred for *vic2*, *vic3*, and *vic7* based on no loss of barrage formation following disruption of one gene at the corresponding loci.

Evidence that the *C. parasitica vic* system restricts mycovirus transmission, while strong, has been only correlative in nature. The results of extensive field studies in Europe and North America are in general agreement that hypovirus transmission and biological control of chestnut blight are more effective when the *C. parasitica* populations exhibit a low diversity of *vic* genotypes (Anagnostakis *et al.* 1986; Heiniger and Rigling 1994; Robin *et al.* 2000, 2009; Milgroom and Cortesi 2004). Laboratory transmission studies have shown *vic* loci-dependent variations in virus transmission, including allele-specific asymmetry, apparently resulting from differences in the rate at which PCD occurs in either or both donor and recipient strains after cell fusion (Cortesi *et al.* 2001; Biella *et al.* 2002). However, the heteroallelic strains used in those studies were not isogenic, raising the possibility of contributions from non-vic genes. The *vic* gene disruption studies reported here and in Choi *et al.* (2012) provide formal confirmation of contributions to

Table 2 PCR-based differentiation of alleles for pseudo *vic* locus at *C. parasitica* genome Scaffold 6: 599,514–606,808

Isolate	Location	Pseudo *vic* allele	Isolate	Location	Pseudo *vic* allele
JA01	Chiyodo, Ibaraki, Japan	1	MD-01	Finzel, MD	1
JA02	Chiyodo, Ibaraki, Japan	PCR failure	MD-05	Finzel, MD	1
JA03	Chiyodo, Ibaraki, Japan	1	MD-07	Finzel, MD	1
JA04	Chiyodo, Ibaraki, Japan	1	MD-09	Finzel, MD	1
JA06	Chiyodo, Ibaraki, Japan	1	MD-11	Finzel, MD	1
JA11	Chiyodo, Ibaraki, Japan	1	MD-16	Finzel, MD	2
JA12	Chiyodo, Ibaraki, Japan	1	MD-18	Finzel, MD	1
JA19	Iwama, Ibaraki, Japan	1	MD-21	Finzel, MD	1
JA20	Iwama, Ibaraki, Japan	2	MD-25	Finzel, MD	1
JA21	Iwama, Ibaraki, Japan	1	MD-28	Finzel, MD	1
JA23	Iwama, Ibaraki, Japan	2	MD-30	Finzel, MD	1
JA60	Yasato, Ibaraki, Japan	1	MD-32	Finzel, MD	2
EU40 (control)		1	MD-34	Finzel, MD	2
EU31 (control)		2	MD-36	Finzel, MD	2

The *C. parasitica* genome Scaffold 6: 599,514–606,808 can be found at http://genome.jgi.doe.gov/Crypa2/Crypa2.home.html. Isolates from Japan and Finzel, Maryland, were used in previous population studies described by Liu and Milgroom (2007) and Milgroom and Cortesi (1999), respectively.

restriction of virus transmission for *vic1a-2*, *vic1b-2*, *vic2-2*, *vic3a-1*, *vic3a-2*, *vic3b-1*, *vic3b-2*, *vic6-1*, *vic6-2*, *pix6-1*, *pix6-2*, and *vic7-2*, representing the five *vic* loci previously implicated.

The *vic* gene disruption studies also strongly support the allorecognition hypothesis rather than the accidental hypothesis of *vic* origins. The former hypothesis proposes that vegetative incompatibility systems arose through positive Darwinian selection because they provide some specific advantages (Saupe 2000; Smith and Lafontaine 2013). One often-mentioned advantage is protection against the transmission of deleterious genetic elements (Caten 1972). Because natural *C. parasitica* populations worldwide are known to be infected by mycoviruses that have a deleterious effect on host functions and reproduction (Anagnostaksis 1982a; Heiniger and Rigling 1994; Milgroom and Cortesi 2004), the molecular identification of the *C. parasitica vic* genes provides new opportunities, not available with *N. crassa* and *P. anseria*, for testing this hypothesis. A major prediction of the allorecognition hypothesis is that the *C. parasitica vic* genes that have been demonstrated to contribute to restriction of mycovirus transmission as a result of the incompatibility reaction would be unlikely to have other biological functions. As reported here and in Choi *et al.* (2012), no phenotypic changes, other than reduced rate (increased virus transmission) or loss of PCD, were detected for disruption mutants of 11 polymorphic genes associated with *vic1*, *vic2*, *vic3*, *vic6*, and *vic7*, consistent with dedicated roles in allorecognition. The molecular

Table 3 Summary of *C. parasitica vic*-associated genes identified at the molecular level

Gene[a]	P/I[b]	Allelic/nonallelic	Protein features	Gene disruption increases virus transmission[c]
vic1a	P	Allelic[d]	HET domain	Yes
vic1b-2	I	Nonelleic[e]	DUF domain	Yes
vic1c-1	I	ND[f]	LTR retrotransposon	ND
vic1d-1	I	ND	HET domain	ND
vic2	P	Nonallelic[e]	Patatin-like phospholipase	Yes
vic2a	P	ND	Sec9-like	ND
vic3a	P	Nonallelic[e]	Hypothetical protein	Yes
vic3b	P	Nonallelic[e]	Life guard-1-like	Yes
vic4-1	I	ND	Protein kinase c-like	NA[g]
vic4-2	I	ND	NACHT + WD40 domains	NA
vic6	P	Nonallelic	HET domain	Yes
pix6	P	Nonallelic	DUF1040 domain	Yes
vic7	P	Nonallelic[e]	HET domain	Yes

[a] Molecular identification of *vic2*, *vic4*, *vic6*, and *vic7* reported in Choi *et al.* (2012). Molecular identification of *vic1* and *vic3* reported in this study. Allele specificity is indicated for idiomorphic genes and not polymorphic genes.
[b] *P*, polymorphic; I, idiomorphic.
[c] Transmission increased when the disrupted strain was paired with a nonmutant strain that is heteroallelic only at the *vic* locus being analyzed, *e.g.*, Δ*vic1a-2* (~~2~~211-22) *vs.* EU31 (1211-22).
[d] Potential allelic interaction that requires *vic1a-1* disruption for confirmation.
[e] Inferred as nonallelic based on the presence of two polymorphic or idiomorphic genes at locus and on the observation that incompatibility reaction is not eliminated when one gene at locus is disrupted.
[f] ND, not determined.
[g] NA, not applicable. Virus transmission is not restricted by allelic differences at *vic4*.

identification of the *C. parasitica vic* loci also provides an unparalleled opportunity to test predictions of diversifying and balanced selection of *vic* gene polymorphism in a fungus under pressure of natural infection by a deleterious pathogen.

The one exception where disruption of a *vic* gene did have additional phenotypic consequences, *i.e.*, disruption of *vic1b-2*, requires further study. The reduced growth, irregular colony morphology, increased asexual sporulation, and reduced virulence exhibited by the Δ*vic1b-2* disruption mutant certainly suggests functional roles for the corresponding gene product in cellular processes other than those for nonself recognition. However, while *vic1b-2* disruption did increase virus transmission if the mutant strain served as a recipient, disruption of the Het-domain gene at this locus, *vic1a-2*, in just one of two heteroallelic strains was sufficient to completely abolish PCD and allowed virus transmission in both directions. This raises questions about the role of *vic1b* in the incompatibility reaction. Does it play an auxiliary role, modifying the activity of *vic1a*? Does it interact with *vic1a*? In analogy with the guard hypothesis in plant disease resistance, does the *vic1b* product serve as a guard of the *vic1a* product and are the phenotypic consequences of *vic1b* gene disruption a result of *vic1a* protein activation in the absence of *vic1b*? All of these possibilities are testable and will be the subject of future studies.

The polymorphism-based comparative genomics approach used to identify the *C. parasitica vic* loci (this study and Choi *et al.* 2012) should have general applicability for identifying fungal allorecognition loci. The availability of a set of genotyped *vic* tester strains and linkage map markers for five of the six *vic* loci was certainly useful in their identification. However, the identification of the *vic3* locus in the absence of linkage marker guides (Figure 4) suggests that manual inspection of sequence read-density plots for polymorphism-related gaps in alignment of resequenced and reference genome sequences will provide a good list of candidate *vic* loci for functional characterization. It is noteworthy that >100,000 polymorphisms were found when comparing the EP155 reference genome sequence and the sequence generated by resequencing strain EP146 (Choi *et al.* 2012). Of these, only 3681 were located in predicted coding regions, and only 2079 of those were predicted to result in nonsynonymous changes in a protein product. Highly polymorphic regions that did not involve repetitive sequence elements, such as the identified *vic* loci, were rare. Of course, the presence of a HET-domain or WD repeat gene in the region of polymorphism would indicate a prime candidate *vic* locus.

The identification of the nonfunctional pseudo *vic* locus on Scaffold 6 (Figure 7 and Figure 8) also indicates that the polymorphism-based comparative genomic approach holds promise for providing insights into the origins and evolution of *vic* loci. The polymorphism, or indel, in this case involved an apparent deletion of a HET-domain gene and of an adjacent GTPase-domain gene. That the difference is due to a deletion rather than an insertion is suggested by the observation that the two flanking direct imperfect repetitive elements present in allele 1 (Figure 8) are replaced by a single chimeric sequence consisting of 598 bp of the left repeat and 304 bp of the right repeat with a G-C base pair replacing a T-A base pair at the breakpoint (Figure S9). Interestingly, this presumptive deletion event is not recent, since it was found in *C. parasitica* field isolates collected in Asia, Europe, and North America (Table 2). Repetitive elements have also been identified associated with a sequence inversion event at the *het-6* locus of *N. crassa* (Micali and Smith 2006). Combined with the LTR retrotransposon associated with the sequence inversion and sequence insertion at the *vic1* locus (Figure 2), these observations provide additional support for the proposal that mobile genetic elements contributed to the origins and evolution of *vic* loci (Smith and Lafontaine 2013). It is anticipated that analysis of the corresponding genomic sequences in species closely related to *C. parasitica*—*e.g.*, *C. radicalis*, *C. nitschkei*, *C. megaspore* (Gryzenhout *et al.* 2006), and *C. naterciae* (Braganca *et al.* 2011)—will provide additional insights into the origins and maintenance of vegetative incompatibility.

The use of hypovirus-infected hypovirulent *C. parastica* strains to control chestnut blight by treating individual cankers on blighted trees has been well demonstrated (Anagnostakis and Kranz 1987) and is used in orchard settings (Heiniger and Rigling 1994) and to preserve chestnut germplasm used in backcross resistance breeding programs (Jacobs *et al.* 2013). Application of the virus-infected strain to the margin of a canker can result in viral transmission and spread of the virus in the recipient strain, resulting in conversion to hypovirulence and shutdown of canker expansion. Such treatment is 100% effective if the donor and recipient strains have identical *vic* genotypes. However, treatment effectiveness decreases as the number heteroallelic *vic* genes increases. The molecular identification of the six genetically defined *vic* loci now provides the opportunity to engineer a universal hypovirus donor strain for effective and efficient treatment of individual blight cankers irrespective of the recipient *vic* genotype. The use of a universal donor strain as a vector for delivery of hypoviruses into a forest ecosystem may also find some enhanced utility for woodland restoration of the American chestnut.

Acknowledgments

This work was supported by National Science Foundation awards DBI-MRI-0821806 (Peter Houde, New Mexico State University, Las Cruces, NM, PI), MCB-1051453 (A.L.D.), and MCB-1051331 (D.L.N.).

Literature Cited

Aanen, D. K., A. J. M. Debets, J. A. G. M. de Visser, and R. F. Hoekstra, 2008 The social evolution of somatic fusion. Bioessays 30: 1193–1203.

Anagnostakis, S. L., 1982a Biological control of chestnut blight. Science 215: 466–471.

Anagnostakis, S. L., 1982b Genetic analysis of *Endothia parasitica*: linkage map of four single genes and three vegetative compatibility types. Genetics 102: 25–28.

Anagnostakis, S. L., 1983 Conversion to curative morphology in *Endothia parasitica* and its restriction by vegetative compatibility. Mycologia 79: 23–37.

Anagnostakis, S. L., 1988 *Cryphonectria parasitica*, cause of chestnut blight. Adv. Plant Pathol. 6: 123–136.

Anagnostakis, S. L., and J. Kranz, 1987 Population dynamics of *Cryphonectria parasitica* in a mixed-hardwood forest in Connecticut. Phytopathology 77: 751–754.

Anagnostakis, S. L., B. Hau, and J. Kranz, 1986 Diversity of vegetative compatibility groups of *Cryphonectria parasitica* in Connecticut and Europe. Plant Dis. 70: 536–538.

Bastiaans, E., A. J. M. Debets, D. K. Aanen, A. D. van Diepeningen, S. J. Saupe *et al.*, 2014 Natural variation of heterokaryon incompatibility gene *het-c* in *Podospora anserina* reveals diversifying selection. Mol. Biol. Evol. 31: 962–974.

Biella, S., M. L. Smith, J. R. Aist, P. Cortesi, and M. G. Milgroom, 2002 Programmed cell death correlates with virus transmission in a filamentous fungus. Proc. Biol. Sci. 269: 2269–2276.

Borges, M. J., M. O. Azevedo, R. Bonatelli, Jr., M. S. S. Felipe, and S. Astolfi-Filho, 1990 A practical method for the preparation of total DNA from filamentous fungi. Fungal Genet. Newsl. 37: 10.

Braganca, H., D. Rigling, E. Diogo, J. Capelo, A. Phillips *et al.*, 2011 *Cryphonectria naterciae*: a new species in the *Cryphonectria-Endothia* complex and diagnostic molecular markers based on microsatellite-primed PCR. Fungal Biol. 115: 852–861.

Caten, C. E., 1972 Vegetative incompatibility and cytoplasmic infections in fungi. J. Gen. Microbiol. 72: 221–229.

Chen, B., G. H. Choi, and D. L. Nuss, 1994 Attenuation of fungal virulence by synthetic infectious hypovirus transcripts. Science 264: 1762–1764.

Choi, G. H., A. L. Dawe, A. Churbanov, M. L. Smith, M. G. Milgroom *et al.*, 2012 Molecular characterization of vegetative incompatibility genes that restrict hypovirus transmission in the chestnut blight fungus *Cryphonectria parasitica*. Genetics 190: 113–127.

Churchill, A. C. L., L. M. Ciufetti, D. R. Hansen, H. D. Van Etten, and N. K. Van Alfen, 1990 Transformation of the fungal pathogen *Cryphonectria parasitica* with a variety of heterologous plasmids. Curr. Genet. 17: 25–31.

Coppin, E., R. Debuchy, S. Arnaise, and M. Picard, 1997 Mating types and sexual development in filamentous ascomycetes. Microbiol. Mol. Biol. Rev. 61: 411–428.

Cortesi, P., and M. G. Milgroom, 1998 Genetics of vegetative incompatibility in *Cryphonectria parasitica*. Appl. Environ. Microbiol. 64: 2988–2994.

Cortesi, P., C. E. McCulloch, H. Song, H. Lin, and M. G. Milgroom, 2001 Genetic control of horizontal virus transmission in the chestnut blight fungus, *Cryphonectria parasitica*. Genetics 159: 107–118.

Dawe, A. L., and D. L. Nuss, 2013 Hypovirus molecular biology: from Koch's postulates to host self-recognition genes that restrict virus transmission. Adv. Virus Res. 86: 109–147.

Debets, A. J. M., and A. J. F. Griffiths, 1998 Polymorphisms in het-genes prevents resource plundering in *Neurospora crassa*. Mycol. Res. 102: 1343–1349.

De Tomaso, A. W., S. V. Nyholm, K. J. Palmeri, K. J. Ishizuka, W. B. Ludington *et al.*, 2005 Isolation and characterization of a protochordate histocompatibility locus. Nature 438: 454–459.

Fournier, E., C. Levis, D. Fortini, P. Leroux, T. Giraud *et al.*, 2003 Characterization *Bc-hch*, the *Botrytis cinerea* homolog of the *Neurospora crassa* het-c vegetative incompatibility locus, and its use as a population marker. Mycologia 95: 251–261.

Ghabrial, S. A., and N. Suzuki, 2009 Viruses of plant pathogenic fungi. Annu. Rev. Phytopathol. 47: 353–384.

Glass, N. L., S. J. Vollmer, C. Staben, R. L. Metzenbereg, and C. Yanofski, 1988 DNAs of the two mating type alleles of *Neurospora crassa* are highly dissimilar. Science 241: 570–573.

Glass, N. L., J. Grotelueschen, and R. L. Metzenberg, 1990 *Neurospora crassa* A mating-type proteins. Proc. Natl. Acad. Sci. USA 87: 4912–4916.

Glass, N. L., D. J. Jacobson, and P. K. Shiu, 2000 The genetics of hyphal fusion and vegetative incompatibility in filamentous ascomycete fungi. Annu. Rev. Genet. 34: 165–186.

Gryzenhout, M., B. Wingfield, and M. Wingfield, 2006 New taxonomic concepts for the important forest pathogens *Cryphonectria parasitica* and related fungi. FEMS Microbiol. Lett. 258: 161–172.

Hall, C., J. Welch, D. J. Kowbel, and N. L. Glass, 2010 Evolution and diversity of a fungal self/nonself recognition locus. PLoS ONE 5: el4055.

Heiniger, U., and D. Rigling, 1994 Biological control of chestnut blight in Europe. Annu. Rev. Phytopathol. 32: 581–599.

Hillman, B. I., R. Shapira, and D. L. Nuss, 1990 Hypovirulence-associated suppression of host functions in *Cryphonectria parasitica* can be partially relieved by high light intensity. Phytopathology 80: 950–956.

Huber, D. H., 1996 Genetic analysis of vegetative incompatibility polymorphisms and horizontal transmission in the chestnut blight fungus *Cryphonectria parasitica*. Ph.D. Thesis, Michigan State University, East Lansing, MI.

Huber, D. H., and D. W. Fulbright, 1994 Preliminary investigations on the effect of individual genes upon the transmission of dsRNA in *Cryphonectria parasitica*, pp. 15–19 in *Proceedings of the International Chestnut Conference*, edited by M. L. Double and W. L. MacDonald. West Virigina University Press, Morgantown, WV.

Iotti, M., A. Rubini, E. Tisserant, A. Kholer, F. Paolocci *et al.*, 2012 Self/nonself recognition in *Tuber melanosporum* is not mediated by a heterokaryon incompatibility system. Fungal Biol. 116: 261–275.

Jacobs, D. F., H. J. Dalgleish, and C. D. Nelson, 2013 A conceptual framework for restoration of threatened plants: the effective model of American Chestnut (*Castanea dentata*) reintroduction. New Phytol. 197: 378–393.

Kerenyi, Z., B. Olah, A. Jeney, L. Hornok, and J. F. Leslie, 2006 The homologue of *het-c* of *Neurospora crassa* lacks vegetative compatibility function in *Fusarium proliferatum*. Appl. Environ. Microbiol. 72: 6527–6532.

Kinsey, J. A., 1990 Tad, a LINE-like transposable element in *Neurospora*, can transpose between nuclei in heterokaryons. Genetics 126: 317–323.

Kubisiak, T. L., and M. G. Milgroom, 2006 Markers linked to vegetative incompatibility (*vic*) genes and a region of high heterogeneity and reduced recombination near the mating type locus (*MAT*) in *Cryphonectria parasitica*. Fungal Genet. Biol. 43: 453–463.

Kuwayama, H., S. Obara, T. Morio, M. Katoh, H. Urushihara *et al.*, 2002 PCR-mediated generation of a gene disruption construct without the use of DNA ligase and plasmid vectors. Nucleic Acids Res. 15: E2.

Lafontaine, D. L., and M. L. Smith, 2012 Diverse interactions mediate asymmetric incompatibility by the *het-6* supergene complex in *Neurospora crassa*. Fungal Genet. Biol. 49: 65–73.

Lan, X., Z. Yao, Y. Zhou, J. Shang, H. Lin *et al.*, 2008 Deletion of the *cpku80* gene in the chestnut blight fungus, *Cryphonectria parasitica*, enhances gene disruption efficiency. Curr. Genet. 53: 59–66.

Liu, Y. C., and M. G. Milgroom, 1996 Correlation between hypovirus transmission and the number of vegetative incompatibility (*vic*) genes different among isolates from a natural population of *Cryphonectria parasitica*. Phytopathology 86: 79–86.

Liu, Y. C., and M. G. Milgroom, 2007 High diversity of vegetative compatibility types in *Cryphonectria parasitica* in Japan and China. Mycologia 99: 279–284.

MacDonald, W. L., and D. W. Fulbright, 1991 Biological control of chestnut blight: use and limitations of transmissible hypovirulence. Plant Dis. 75: 656–661.

Margulies, M., M. Egholm, W. E. Altman, S. Attiya, J. S. Bader *et al.*, 2005 Genome sequencing in microfabricated high-density picolitre reactors. Nature 437: 376–380.

Medzhitov, R., and C. A. Janeway, Jr.., 2002 Decoding the patterns of self and nonself by the innate immune system. Science 296: 298–300.

Meselson, M., and R. Yuan, 1968 DNA restriction enzyme from E. coli. Nature 217: 1110–1114.

Micali, C. O., and M. L. Smith, 2006 A nonself recognition gene complex in *Neurospora crassa*. Genetics 173: 1991–2004.

Milgroom, M. G., and P. Cortesi, 1999 Analysis of population structure of the chestnut blight fungus based on vegetative incompatibility genotypes. Proc. Natl. Acad. Sci. USA 96: 10518–10523.

Milgroom, M. G., and P. Cortesi, 2004 Biological control of chestnut blight with hypovirulence: a critical analysis. Annu. Rev. Phytopathol. 42: 311–338.

Nasrallah, J. B., 2005 Recognition and rejection of self in plant self-incompatibility: comparisons to animal histocompatibility. Trends Immunol. 26: 412–418.

Nuss, D. L., 1992 Biological control of chestnut blight: an example of virus-mediated attenuation of fungal pathogenesis. Microbiol. Rev. 56: 561–576.

Nuss, D. L., 2005 Hypovirulence: mycoviruses at the fungal-plant interface. Nat. Rev. Microbiol. 3: 632–642.

Nydam, M. L., and A. W. De Tomaso, 2011 Creation and maintenance of variation in allorecognition loci: molecular analysis in various model systems. Front. Immunol. 2: 79.

Pal, K., A. D. van Diepeningen, J. Varga, R. F. Hoekstra, P. S. Dyer *et al.*, 2007 Sexual and vegetative compatibility genes in the aspergilla. Stud. Mycol. 59: 19–30.

Pontecorvo, G., 1956 The parasexual cycle in fungi. Annu. Rev. Microbiol. 10: 393–400.

Powell, W. A., 1995 Vegetative incompatibility and mycelial death of *Cryphonectria parasitica* detected with a pH indicator. Mycologia 87: 738–741.

Rayner, A. D. M., 1996 Interconnectedness and individualism in fungal mycelia, pp. 193–232 in *A Century of Mycology*, edited by B. C. Sutton. University Cambridge Press, Cambridge, UK.

Robin, C., C. Anziani, and P. Cortesi, 2000 Relationship between biological control, incidence of hypovirulence, and diversity of vegetative incompatibility types of *Cryphonectria parasitica* in France. Phytopathology 90: 730–737.

Robin, C., X. Capdeville, M. Martin, C. Traver, and C. Colinas, 2009 *Cryphonectria parasitica* vegetative compatibility type analysis of populations in south-western France and northern Spain. Plant Pathol. 58: 527–535.

Rosengarten, R. D., and M. L. Nicotra, 2011 Model systems of invertebrate allorecognition. Curr. Biol. 21: R82–R92.

Saupe, S. J., 2000 Molecular genetics of heterokaryon incompatibility in filamentous ascomycetes. Microbiol. Mol. Biol. Rev. 64: 489–502.

Saupe, S., C. Descampus, B. Turcq, and J. Begueret, 1994 Inactivation of the *Podospora anserina* vegetative incompatibility locus *het-c*, whose product resembles a glycolipid transferase protein, drastically impairs ascospore production. Proc. Natl. Acad. Sci. USA 91: 5927–5931.

Smith, M. L., and D. Lafontaine, 2013 The fungal sense of nonself, pp. 9–21 in *Neurospora: Genomics and Molecular Biology*, edited by D. Kasbeker, and K. McClusky. Horizon Scientific Press, Norfolk, UK.

Smith, M. L., O. C. Micali, S. P. Hubbard, N. Mir-Rashed, D. J. Jacobson *et al.*, 2000 Vegetative incompatibility in the het-6 region of *Neurospora crassa* is mediated by two linked genes. Genetics 155: 1095–1104.

Smith, M. L., C. C. Gibbs, and M. G. Milgroom, 2006 Heterokaryon incompatibility function of barrage-associated vegetative incompatibility genes (*vic*) in *Cryphonectria parasitica*. Mycologia 98: 43–50.

Spiering, M. J., J. R. Faulkner, D.-X. Zhang, C. Machado, R. B. Grossman *et al.*, 2008 Role of the LolP cytochrome P450 monooxygenase in loline alkaloid biosynthesis. Fungal Genet. Biol. 45: 1307–1314.

Staben, C., and C. Yanofsky, 1990 *Neurospora crassa* a mating-type region. Proc. Natl. Acad. Sci. USA 87: 4917–4921.

Van Alfen, N. K., R. A. Jaynes, S. L. Anagnostakis, and P. R. Day, 1975 Chestnut blight: biological control by transmissible hypovirulence in *Endothia parasitica*. Science 189: 890–891.

Van der Nest, M. A., A. Olson, M. Lind, H. Velez, K. Dalman *et al.*, 2014 Distribution and evolution of het gene homologs in the basidiomycota. Fungal Genet. Biol. 54: 45–57.

Van Diepeningen, A. D., K. Pal, T. A. J. van der Lee, R. F. Hoekstra, and A. J. M. Debets, 2008 The *het-c* heterokaryon incompatibility gene in *Aspergillus niger*. Mycol. Res. 113: 222–229.

Zhang, D.-X., H.-L. Lu, X. Liao, R. J. St. Leger, and D. L. Nuss, 2013 Simple and efficient recycling of fungal selectable marker genes with the Cre-*loxP* recombination system via anastomosis. Fungal Genet. Biol. 61: 1–8.

Communicating editor: J. Heitman

GENETICS

Supporting Information
http://www.genetics.org/lookup/suppl/doi:10.1534/genetics.114.164574/-/DC1

Vegetative Incompatibility Loci with Dedicated Roles in Allorecognition Restrict Mycovirus Transmission in Chestnut Blight Fungus

Dong-Xiu Zhang, Martin J. Spiering, Angus L. Dawe, and Donald L. Nuss

DOI: 10.1534/genetics.114.164574

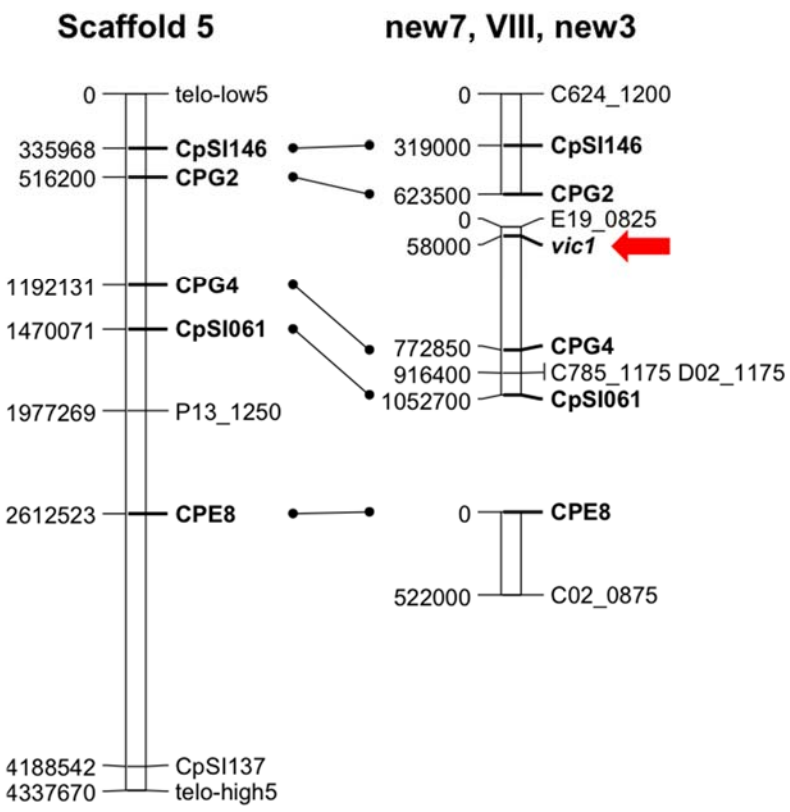

Figure S1 Alignment of *C. parasitica* genetic linkage groups containing the *vic1* locus (red arrow) and associated linkage markers [modified from Kubisiak and Milgroom, (2006) by addition of simple sequence repeat markers (bold) as indicated in Choi et al. (2012)] with Scaffold 5 of version 2 of the *C. parasitica* reference genome sequence assembly (http://genome.jgi.doe.gov/Crypa2/Crypa2.home.html). The estimated physical distance (in base pairs) of each marker from the end of the linkage group (shown on the left side) was calculated using an estimate of 1cM = 14.5 kb (Kubisiak and Milgroom, 2006). Markers linking the physical and genetic maps are indicated by connecting lines.

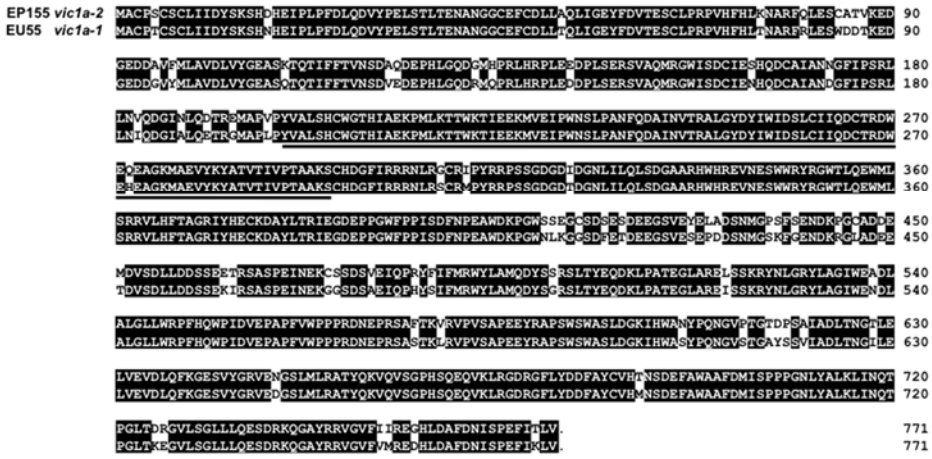

Figure S2 Amino acid sequence alignment of the HET-domain–containing proteins present at the *vic1* alleles in strains EP155 (*vic1a-2*) and EU55 (*vic1a-1*). The alignment was performed with the MUltiple Sequence Comparison by Log Expectation (MUSCLE) method at EMBL-EBI (http://www.ebi.ac.uk/Tools/msa/muscle/). Although similar (91% identical) in sequence, >70 amino acid polymorphisms can be seen throughout the entire alignment of the predicted proteins. The conserved HET domain (pfam06985) present in both proteins is underlined. Identical amino acids are indicated in white on black background.

Figure S3 Amino acid sequence alignment of the clavaminate synthase–like proteins present at the *vic1* alleles in strains EP155 (*vic1-2*) and EU55 (*vic1-1*). The alignment was performed with MUSCLE. Note that the two proteins are very similar in sequence (96% identical and 98% similar), displaying 16 polymorphic amino acids, most of which are located at the C-terminal regions of the proteins. A conserved 2OG-Fe(II) oxygenase superfamily domain (at amino acids 6–126; pfam14226) and a conserved Fe(2+) 2-oxoglutarate dioxygenase domain (at amino acids 174–281; Prosite PS51471) are present in both proteins and are underlined. Identical amino acids are indicated in white on black background.

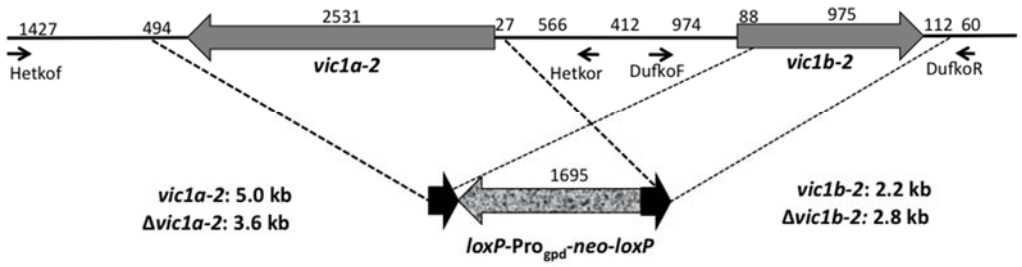

Figure S4 Disruption of candidate *vic1*-associated genes. Disruption of *vic1a-2* in strain DK80 involved replacing the entire CDS (solid grey box) extending from 27 nts upstream of the start codon to 494 nts downstream of the stop codon with a 1.7-kb *loxP*-flanked G418 resistance (neomycin phosphotransferase) gene driven by the *Cochliobolus heterostrophus* glyceraldehyde-3-phosphate dehydrogenase promoter (*loxP*-Pro$_{gpd}$-*neo*-*loxP*) (Zhang et al., 2013). Disruption of *vic1b-2* in strain DK80 involved replacing most of the CDS extending from 88 nts downstream of the start codon to 112 nts downstream of the stop codon with the 1.7 kb l*oxP*-Pro$_{gpd}$-*neo*-*loxP* cassette. The GPD promoter/neomycin phosphotransferase cassette is indicated by the patterned shaded box. The thick black arrows indicate the locations of the *loxP* sites. The thin arrows indicate the locations of the *vic1a-2*-specific primers Hetkof and Hetkor and *vic1b-2*-specific primers DufkoF and DufkoR. Primer sequences are shown in Table S1. The predicted sizes of the PCR amplicons generated by the Hetkof/Hetokr primer pair for the intact and disrupted (Δ*vic1a-2*) *vic1a-2* genes are shown at the left. The predicted sizes of the PCR amplicons generated by the *vic1b-2*-specific DufkoF/DufkoR primer pair for the intact and disrupted (Δ*vic1b-2*) *vic1b-2* genes are shown at the right. The sizes in nucleotides of elements within the *vic1-2* locus are indicated at the top of the figure. The distances are not drawn to exact scale.

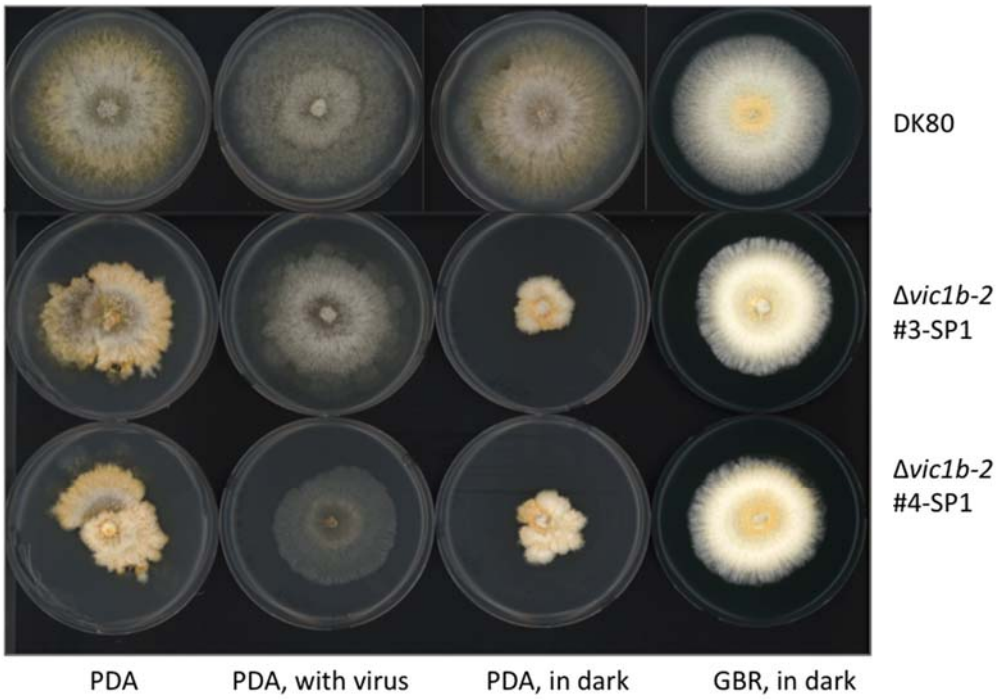

Figure S5 Colony morphology of the *vic1b-2* disruption mutant strain. Colonies of the parental strain DK80 are shown on the top row and colonies of two single-spored Δ*vic1b-2* mutant strains generated from independent transformation events are shown in the middle and bottom rows. Photographs were taken after seven days of growth. When grown on standard PDA medium (left-most column), the Δ*vic1b-2* mutant strains grew at a slower rate than the parental DK80 strain and exhibited a non-uniform, sectored colony morphology with very uneven margins. These differences in growth rate and colony morphology were partially relieved when the parental and mutant strains were infected with hypovirus CHV-1/EP713 (second column from left), but was accentuated when the strains were grown in the dark (third column from the left). The slow growth and altered colony morphology of the mutant strains were significantly ameliorated (right-most column) when grown on a rich media (GBR: PDA supplemented with 7g/L malt extract, 2g/L yeast extract, 0.8 g/L tannic acid, 50mg/L Bromocresol Green, 20g/L additional agar and 12 drops of Tween 20; modified from Powell, 1995).

Figure S6 Amino acid sequence alignment of the hypothetical proteins present at the *vic3* alleles in strains EP155 (*vic3a-1*) and EU55 (*vic3a-2*). The alignment was performed with MUSCLE. Note that the two protein sequences contain several stretches of polymorphic amino acids and are only 46% identical (60% similar). Searches of the conserved domain database at NCBI and the Prosite database failed to detect any conserved domains or signature motifs in the two protein. Identical amino acids are indicated in white on black background.

Figure S7 Amino acid sequence alignment of the glutamate receptor-like (Lifeguard 1-like) proteins present at the *vic3* alleles in strains EP155 (*vic3b-1*) and EU55 (*vic3b-2*). The sequence alignment was performed with MUSCLE. Note that both proteins contain several glycine- and glutamine-rich repeats (underlined with solid line) and are similar in sequence (85% identical and 87% similar), displaying 15 polymorphic amino acid sites, most of which are located at the N- and C-terminal regions of the two proteins. The *vic3-2* protein in EU55 contains a 2Fe-2S ferredoxin-type iron-sulfur binding signature at amino acids 83–91 ("CLEAMCAAC"; Prosite pattern PS00197, underlined with dashed line) that is absent in the predicted protein from the *vic3-1* allele. Identical amino acids are indicated in white on black background.

Fig. S8A

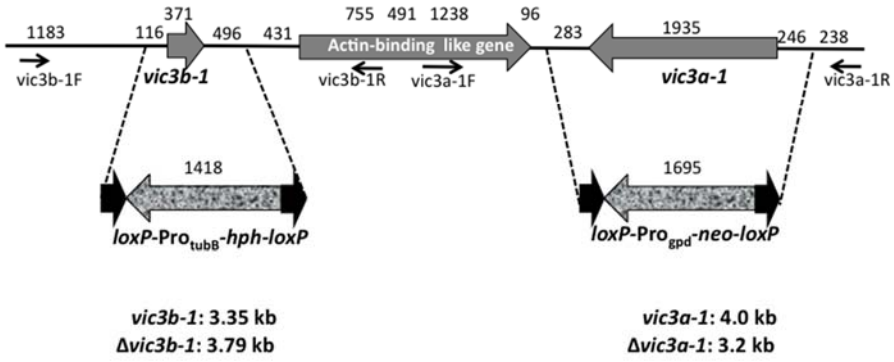

Fig. S8B

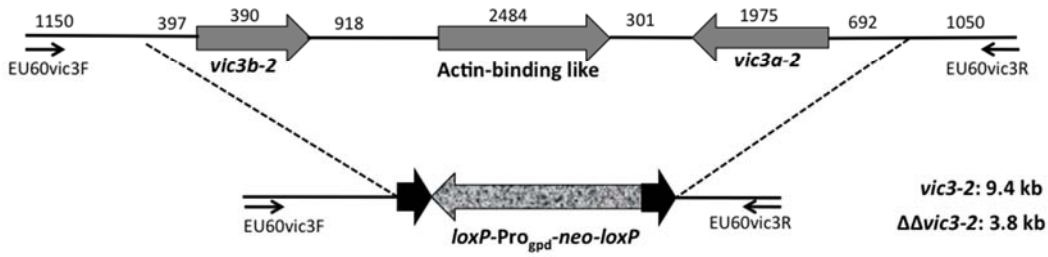

Figure S8 Disruption of candidate *vic3*-associated genes. (A) Disruption of *vic3a-1* involved replacing the entire CDS extending from 246 nts upstream of the start codon to 283 nts downstream of the stop codon with the *loxP*-Pro$_{gpd}$-*neo-loxP* cassette. The conventions used for Figure S4 are used in this figure. The predicted sizes of the PCR amplicons generated by the *vic3a-1*-specific primer pair vic3a-1F/vic3a-1R for the intact and disrupted (Δ*vic3a-1*) genes are indicated at the bottom right of the figure. Disruption of *vic3b-1* involved use of the *loxP*-Pro$_{tubB}$-*hph-loxP* cassette to replace the entire CDS extending from 116 nts upstream of the start codon and 496 nts downstream of the stop codon. The predicted sizes of the PCR amplicons generated by the *vic3b-1*-specific primer pair vic3b-1F/vic3b-1R for the intact and disrupted (Δ*vic3b-1*) genes are indicated at the bottom left of the figure. The double *vic3a-1*/*vic3b-1* mutant in strain DK80 (ΔΔ*vic3-1*) was generated by disrupting the *vic3b-1* gene in the DK80Δ*vic3a-1* mutant strain, as was done for generation of the Δ*vic3b-1* single mutant strain shown here. The actin binding-like gene located between *vic3a-1* and *vic3b-1* was not disturbed in this double mutant. (B) Disruption of both *vic3a-2* and *vic3b-2* in strain EU60 (EU60 ΔΔ*vic3-2*). In this case the *loxP*-Pro$_{gpd}$-*neo*-l*oxP* cassette was used to replace a 7.2 kb portion of the candidate *vic3-2* locus extending from 397 nts upstream of the *vic3b-2* start codon and 692 nts upstream of the *vic3a-2* start codon. The deleted region included an ORF encoding a conserved actin-binding-like protein located between *vic3a-2* and *vic3b-2*. The predicted sizes of the PCR amplicons generated by the EU60vic3F and EU60vic3R primer pair for the intact and disrupted ΔΔ*vic3-2* genes are shown at the right.

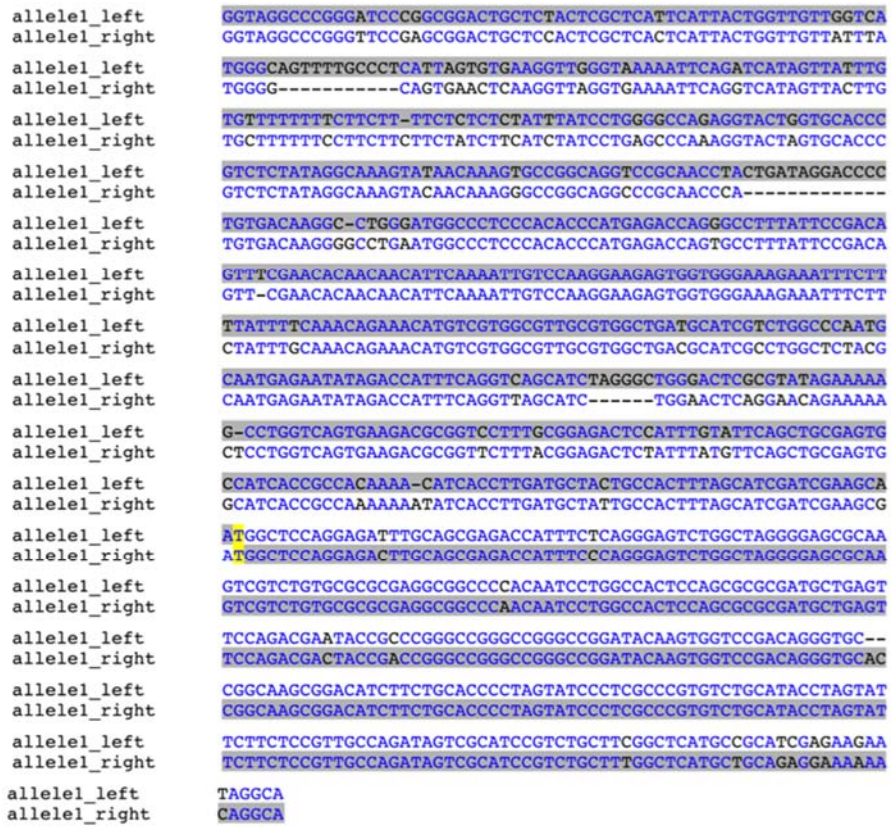

Figure S9 Alignment of the direct repeats flanking the pseudo *vic* locus located on Scaffold 6 spanning positions 599514-606808 in the EP155 reference genome assembly. The sequence of the left repeat is shown on the top line and the sequence of the right repeat on the bottom line. Sequence identity is indicated in blue and heterogeneity is indicated in black. The sequence of the chimeric repeat found in allele 2 is indicated by the grey shading of the corresponding left and right repeat sequences. The T residue indicated in yellow is re-laced by a G residue in the chimeric repeat.

Table S1 Oligonucleotide PCR primers used in this study

Primer	Sequence (5'-3')	Note
Hetkof	CAC TCA ACC ATC GCA CTG AGC AGC ATT TCT CTG A	For analysis of *vic1a-2* knockout
Hetkor	AAC TGA AAC GAT GCA AGA CTG CGT GTT CGA GAT	
DufkoF	AAG AGC CAC GCA TGA AAT GAT GGT CAC AAG T	For analysis of *vic1b-2* knockout
DufkoR	TGA ATA TCC AAC TGC GGT GGA CCG TAC CTG	
vic3a-1F	TAC ATT TGC GGA CCA AGG AGG GAA GAC TCC	For analysis of *vic3a-1* knockout
vic3a-1R	GAG AGA GGG CAG GAT TCT ACT ACC ACT TAC ATG C	
vic3b-1F	CAG ACT CGA ATC GTA TCG AAG AGA ACC AGC	For analysis of *vic3b-1* knockout
vic3b-1R	GGC TGA CTC GAC TTT CTC GAT CTG TG	
EU60vic3F	AGG CAA CCA AGA CTT CTA AAC ACC ATC	For analysis of EU60 *vic3* knockout
EU60vic3R	CTC CAT ACT AAT GGA AGG CAA CCT CAT AA	
EU31Pseudo(d)	GAC CGC GGA TAC ATG GTA AAA GC	For population assay in determining pseudo *vic* allele by the presence/absence of left repeat, GTPase-domain containing gene, Het-domain containing gene, or the chimeric repeat found in strain EU31.
EU31Pseudo(u)	AGG AGG TCA CCG TCA TCT GTG AAA	
PseudoRPT1(d)	AGG ACG TTG ATC AGC TGG TGA TGC	
PseudoRPT1(u)	GGG ACC TCA ACC TCG TAT CAT TCC TG	
PseudoGTP(d)	AAT GGC TGG GCT TGG GTC CTC T	
PseudoGTP(u)	TGG TCG ACT GTG AGG AAG CAG GC	
PseudoHET(u)	GTG GGC TTT GAT GGG TAC TT	
PseudoHET(d)	GTG GAG AGC CAC TCA TCT TTA C	